

pubs.acs.org/Macromolecules Article

Effects of Asymmetric Molecular Architecture on Chain Stretching and Dynamics in Miktoarm Star Copolymers

Thomas Kinsey, Emmanuel Urandu Mapesa, Weiyu Wang, Kunlun Hong, Jimmy Mays, S. Michael Kilbey, II, and Joshua Sangoro*



Cite This: *Macromolecules* 2021, 54, 183–194



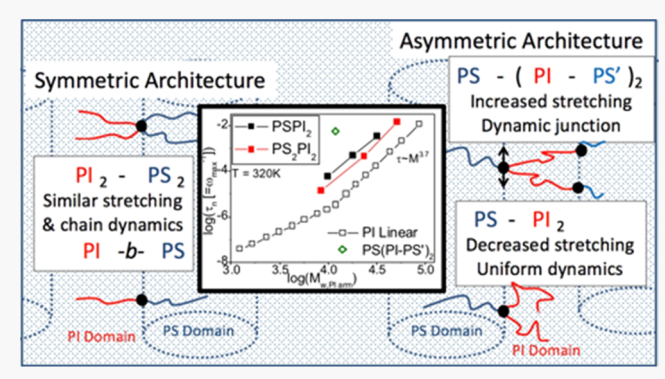
ACCESS

Metrics & More

Article Recommendations

s Supporting Information

ABSTRACT: We use broad-band dielectric spectroscopy (BDS) and small-angle X-ray scattering (SAXS) to investigate the impact of architectural asymmetry in the miktoarm star copolymer on the dielectric polymer relaxations. The miktoarm copolymers studied contain one or two polystyrene (PS) chains of constant molecular weight and two identical poly(cis-1,4-isoprene) (PI) chains with varied molecular weights. Using the chains in the PI block as dielectric probes, we find that the architecturally asymmetric miktoarm star copolymer systems (PSPI₂) feature distributions in chain relaxation times and dielectric relaxation strengths that are not dependent on molecular weight or morphology, in stark contrast to the effects of morphological confinement observed for symmetric diblock systems (PS-b-PI or PS₂PI₂). Along with



evidence from the SAXS measurements regarding phase separation, these results are attributed to influences from chain stretching within the framework of the Gaussian chain model for block copolymer systems. As such, the molecular architecture in block copolymers happens to be a versatile handle to control polymer chain dynamics and, ultimately, the macroscopic physicochemical properties in architecturally complex polymers.

INTRODUCTION

In recent years, increased attention has been given to architecturally complex block copolymers (BCPs) due to the remarkable properties that are attributed, either directly or indirectly, to the special connectivity of the polymer chains. 1-3 Advances in synthesis techniques have afforded precise control over the BCP chain topology, which add molecular architecture as an additional molecular handle to tune the properties of these BCP materials. 4-9 One such architecture is the miktoarm star copolymer, which comprises two or more blocks containing multiple homopolymer chains, or "arms", that are covalently connected at a central junction point. 10,11 A particularly notable feature of the asymmetric miktoarm star copolymer (e.g., AB_n, which has one arm of polymer "A" as a block and "n" arms of polymer "B" as a block) is the reduced domain sizes that are formed during self-assembly with highmolecular-weight blocks compared to those of linear diblock copolymers with similar block molecular weights. 12 Additionally, intricate self-assembled morphologies that are less accessible to or not possible for linear BCPs, such as "brick and mortar", Frank-Kasper σ , and A15 morphologies, have been reported to form due to architectural asymmetry in the miktoarm star copolymer. ^{13–21} In addition to the broad-range morphologies, BCPs with the miktoarm star architecture have also displayed superior macroscopic physical properties

compared to their linear counterparts, such as increased Young's modulus, elastic recovery, and enhanced ionic conductivity. ^{14,20,22–34} The enhanced material properties observed for the miktoarm star copolymers likely arise from contributions of the molecular architecture to morphology and macroscopic dynamics. Although the dynamics of the polymer chains and segments within each block, which ultimately govern the macroscopic properties, are extensively reported for linear BCP systems, ^{35,36} the possible correlations between architecture and dynamics in BCPs with complex architectures remain speculative due to lack of systematic experimental data. In this study, we investigate the relationships between BCP molecular architecture and dynamics and make inferences about the nature of chain stretching as well as interfacial energies as functions of the self-assembled phase separation and block molecular weights.

This work employs broad-band dielectric spectroscopy (BDS) to investigate the dynamics of poly(cis-1,4-isoprene)

Received: August 11, 2020 Revised: December 3, 2020 Published: December 24, 2020





Table 1. Details of the Miktoarm Star Copolymers Investigated in This Study

		molecular weight (kg/mol)						
architecture ID	sample ID	$M_{ m w_{PS,arm}}$	$M_{ m w_{PS,block}}$	$M_{_{ m Wpl,arm}}$	$M_{ m w_{PI,block}}$	$M_{_{ m WPS'arm}}$	$\phi_{ ext{PI}}{}^a$	D^{b}
PSPI ₂	18k-10k ₂	18	18	10	20		0.565	1.05
	$18k-18k_2$	18	18	18	36		0.7	1.02
	$18k - 32k_2$	18	18	32	64		0.806	1.01
PS_2PI_2	$16k_2 - 9k_2$	16	32	9	18		0.396	1.04
	$16k_2 - 24k_2$	16	32	24	48		0.636	1.01
	$16k_2 - 52k_2$	16	32	52	104		0.791	1.08
$PS(PI-PS')_2$	$18k(12k-3k')_2$	18	24	12	24	3	0.538	1.06

^aTotal volume fraction of PI in polymer by $x(x+y)^{-1}$, where $x=M_{w_{Pl,block}}\rho_{Pl}^{-1}$ and $y=M_{w_{Pl,block}}\rho_{PS}^{-1}$ with $\rho_{Pl}=0.83$ g/cm³ and $\rho_{PS}=0.969$ g/cm³. ^bD denotes polydispersity index.

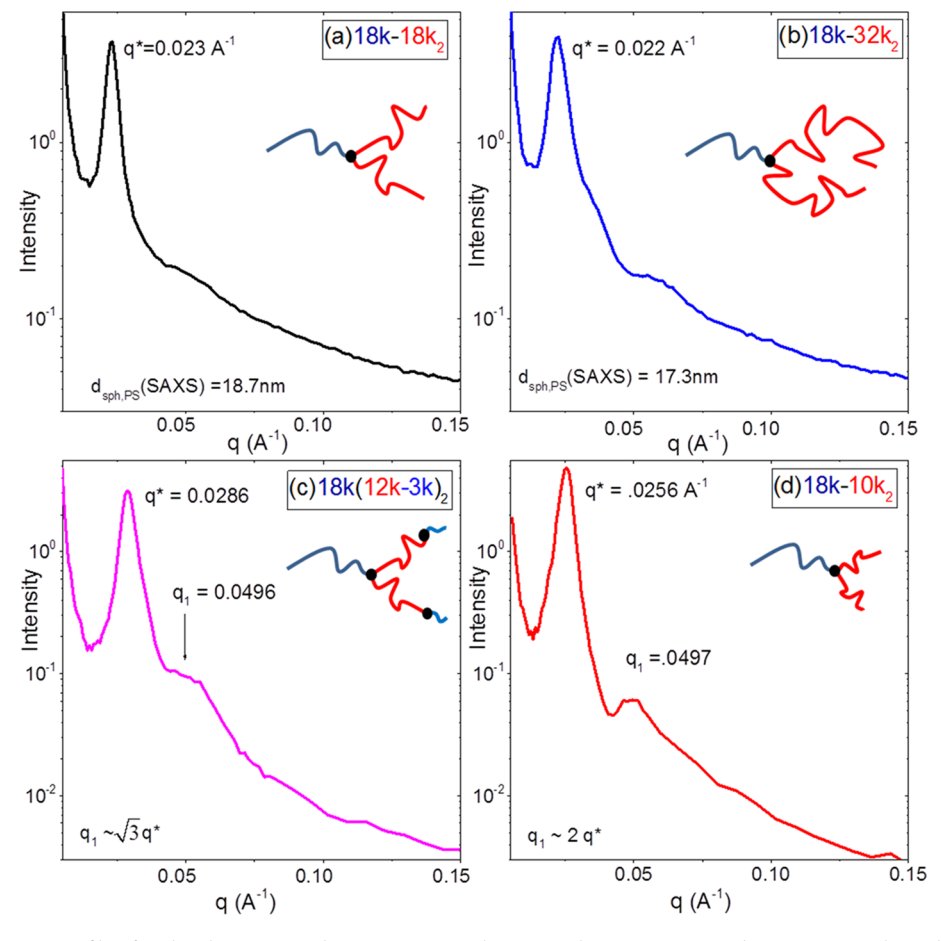


Figure 1. SAXS scattering profiles for the three-arm miktoarm star copolymers with intensities in arbitrary units. The $18k-18k_2$ and $18k-32k_2$ polymers (a, b) adopt a spherical PS morphology with similar PS domain sizes. The $18k(12k-3k')_2$ polymer (c) forms PS cylinders. The $18k-10k_2$ polymer forms lamellae and was published previously and reproduced with permission. A sketch of each polymer architecture is the inset in each plot, with the blue indicating PS blocks and red indicating the PI block. The error associated with the determination of the peak q values is ± 0.0004 Å⁻¹.

(PI) chains and segments in seven miktoarm star copolymers with glassy polystyrene (PS) counterblocks. The polymers studied include three symmetric (A_2B_2) and three asymmetric (AB_2) miktoarm polymers, where "A" refers to the polystyrene [PS] block and "B" refers to the polyisoprene [PI] block, and the PI volume fraction $\phi_{\rm PI}$ is also systematically varied. The self-assembled microstructures and domain length scales are measured using small-angle X-ray scattering (SAXS). We observe that the architecturally asymmetric miktoarm star copolymer systems (PSPI₂) feature distributions in chain relaxation times and dielectric relaxation strengths that are not

dependent on molecular weight or morphology, in stark contrast to the effects of morphological confinement observed for symmetric diblock systems (PS-b-PI or PS₂PI₂). This disparity is argued to be due to reduced energies of chain stretching for the asymmetric systems.

■ MATERIALS AND METHODS

Seven miktoarm star copolymers are investigated in this study: three with the three-arm miktoarm architecture $PSPI_2$, three featuring the four-miktoarm star architecture PS_2PI_2 , and one with the three-arm miktoarm architecture $PS(PI-PS')_2$ with one arm of PS connected to

two diblock copolymer arms PI-PS'. PS' indicates a different molecular weight from that of the main PS block. The main physical characteristics of each copolymer are listed in Table 1. All of the polymers were prepared by anionic polymerization in all-glass reactors with break-seals, distilled benzene as the solvent, and butyl-lithium as the initiator, as previously reported. 4,7,8 These conditions are known to generate PI with high cis-1,4 microstructure (70% cis-1,4, 23% trans-1,4, and 7% 3,4) exhibiting monomeric dipole alignment converging to the primary junction point with the PS block.⁵ Respective chlorosilane linking agents were used to control the chain topology in the miktoarm star copolymers. 4,37 Absolute molecular weights were determined using size exclusion chromatography (Agilent 1260 Infinity II GPC, 1.0 mL/min tetrahydrofuran (THF) mobile phase at 25 °C) with a Wyatt Dawn Heleos 8 multiangle light scattering detector, ViscoStar III, and an Optilab T-rEX from typical polystyrene standards and appropriate refractive index increments (dn/dc). It is worth noting that the PS block of the PSPI₂ copolymers has been isotopically substituted (deuterium for hydrogen) for possible future neutron scattering and ¹H NMR studies. Differences between deuterated and nondeuterated PS have been shown to be negligible in self-assembled phase separation and in the dielectric dynamic glass-transition temperature of deuterated PS ($T_{\rm g}\sim105$ $^{\circ}{\rm C}).^{38,39}$

Small-angle X-ray scattering (SAXS) measurements were performed using an SAXLab Ganesha instrument with a 50 kV Cu Xenocs Genix ULD point source and a 170 μ m pixel, 20 Hz Dectris Pilatus 300k detector at 25 °C. The samples for SAXS measurements were hot-pressed under a N₂ atmosphere at 150 °C for 20 min to form a polymer film of ~100 μ m thickness, annealed for 48 h at 430 K under N₂, then cooled to room temperature, and sandwiched between two layers of Kapton tape. The scattering profile of Kapton was directly subtracted from the measured spectrum of each sample as a background, assuming additivity of the corresponding intensities.

A Novocontrol high resolution Alpha dielectric analyzer equipped with a Quatro Cryosystem temperature control was employed to perform dielectric measurements with an applied electric field of 0.5 V in a frequency range of 10^{-1} – 10^{6} Hz at temperatures of 220 K $\leq T \leq$ 400 K at 10 \pm 0.2 K steps. The polymer films were prepared in the same manner as the SAXS samples, but rather than being sandwiched between Kapton tape, they were inserted between two 10 mm brass electrodes with a fixed spacing achieved using two 100 μ m diameter silica rods. The polymers were annealed in the cryostat under a N2 atmosphere at 430 K for >18 h with constant isothermal dielectric measurement until no change to the dielectric spectrum was observed, which indicated successful thermal equilibration. The polymers were then cooled to 290 K, and the dielectric response was measured. In this study, only the dielectric data at $T \leq 360$ K are presented and discussed. Due to the high $T_{\rm g}$ of the PS block, contributions from its segmental dynamics at $T \le \frac{5}{3}60$ K occur at frequencies slower than our experimental spectral window (<10⁻¹ Hz), allowing access to chain and segmental dynamics of the PI blocks tethered to the glassy PS interface.

RESULTS AND DISCUSSION

Microstructural Characterization by Small-Angle X-ray Scattering (SAXS). Figure 1 shows the SAXS profiles for the $18k-10k_2$, $18k-18k_2$, $18k-32k_2$, and $18k(12k-3k')_2$ polymers plotted *versus* the scattering vector, q. The SAXS profiles of the symmetric four-arm miktoarm copolymers are given in Part A of the Supporting Information. The $18k-10k_2$ and $16k_2-24k_2$ copolymers form lamellar morphologies with domain spacings of 24.6 and 33.2 nm, respectively, as previously reported. From Figure 1, the $18k-18k_2$ and $18k-32k_2$ copolymers appear to self-assemble into spherical PS morphologies in a continuous matrix of PI. Transmission electron microscopy (TEM) images (see Part A of the Supporting Information for details) confirm the assignment

of the morphologies and reveal that, in addition to PS spheres, some cylindrical domains are also observed for the 18k-18k₂ polymer. The mean diameters of these spherical PS domains are \sim 18 \pm 1.2 nm for both systems as calculated using the expression $d_{\rm sph,PS}({\rm SAXS}) = (4\pi/q^*)(2\phi_{\rm Pl}/\pi\sqrt{3})$, where q^* is the scattering vector of the first Bragg peak.⁴¹ The spacing between PS spheres and an extent of long-range order is increased for the 18k-32k2 copolymer as indicated by the SAXS peaks at higher q values and TEM images. For the final two PS₂PI₂ miktoarm copolymers, the microstructures are interpreted as oriented PI spheres for 16k2-9k2 and PS cylinders for 16k2-52k2 (see Figures S2 and S3). In Figure S4, the *q** values are observed to decrease with increasing PI block molecular weight for both PS2PI2 and PSPI2 architectures, but q* decreases faster with molecular weight for the four-arm miktoarm copolymers in agreement with previous reports of smaller domain spacings observed for the asymmetric miktoarm architecture. 12,

The 18k(12k-3k')₂ copolymer forms PS cylindrical morphology as indicated by the higher-order SAXS peak at q = $\sqrt{3}q^*$ in Figure 1c. For linear PS-PI diblock copolymers with $\phi_{\rm PI}$ = 0.5, lamella structures are typically expected. However, the $A(BA')_n$ architecture has previously been shown to form cylinders of the A block for $\phi_{\rm B}=0.5.^{22,31,43}$ To compare the $18k(12k-3k')_2$ copolymer to similar polymers from the literature, the block-asymmetry parameter ($\tau_{\rm bi} = M_{\rm PS}/$ $[M_{\rm PS} + M_{\rm PS'}]$), which quantifies end-block bidispersity of the PS and PS' chains, is calculated to be τ_{bi} = 0.856. This value suggests that there is no deflection in the cylinder-gyroid phase transition region and corroborates our assignment of the higher-order SAXS peak to the formation of cylindrical morphology for the $18k(12k-3k')_2$ polymer. 31,44,45 Comparing the two three-arm miktoarm star copolymers with $\phi_{\rm PI}$ ~ 0.5 in Figure 1c,d, it is interesting that the q^* for 18k(12k-3k')2 is larger than that of the 18k-10k2 polymer, corresponding to a smaller distance between PS domains in the $18k(12k-3k')_2$ polymer even with a larger-molecularweight PI block. This disparity inevitably implies that the PI chains are more stretched across the PI block in the 18k(12k-3k')₂ system. This picture is analogous to that of the wellstudied PI chains in a PS-PI-PS triblock copolymer and will be discussed in more detail in the context of dielectric relaxations for the 18k(12k-3k')₂ copolymer in the Dynamics and Structure of the PS(PI-PS')2 Miktoarm Architecture (BDS and SAXS) section. 46

Dynamics for Symmetric PS_2PI_2 and Asymmetric $PSPI_2$ Architectures. For dynamics of the PI with *cis*-1,4 isomeric chemical structure, which is considered a model type-A polymer, the time-dependent dielectric response function $\Phi(t)$ is related to the complex dielectric function ε^* by

$$\varepsilon^* - \varepsilon_{\infty} = -\Delta\varepsilon \int_0^{\infty} \frac{\mathrm{d}}{\mathrm{d}t} \mathbf{\Phi}(t) \, \mathrm{e}^{-\mathrm{i}2\pi f t} \, \mathrm{d}t \tag{1}$$

where ε_{∞} is the high-frequency (unrelaxed) value of the real part of the dielectric function, $\Delta\varepsilon$ is the dielectric relaxation strength, and f is the frequency of the applied electric field. The alignment of the monomeric dipole moments within the backbone of a type-A chain is such that they may be separated mathematically into vectors that are perpendicular (μ^{\perp}) and parallel (μ^{\parallel}) to the chain contour. The imaginary part of the complex dielectric function $\varepsilon''(f)$ of PI, the averaged polarization responses of μ^{\perp} are observed as a high-frequency, low-temperature segmental process (i.e., α -relaxation) and the

summation of the individual dielectric relaxations of μ^{\parallel} are observed as the normal mode (*i.e.*, chain) relaxation at lower frequencies. When the time scales of these two relaxations are well separated, $\Phi(t)$ is described by a linear combination of the normalized autocorrelation function of the polarizations of the nth and mth segmental dipole vectors separated into μ^{\perp} and μ^{\parallel} portions across all chains by

$$\mathbf{\Phi}(t) = \sum_{i} \frac{\sum_{n} \sum_{m} \langle \mu_{i}^{\parallel}(n; 0) \cdot \mu_{i}^{\parallel}(m; t) \rangle + \sum_{n} \sum_{m} \langle \mu_{i}^{\perp}(n; 0) \cdot \mu_{i}^{\perp}(m; t) \rangle}{\sum_{n} \sum_{m} \langle \mu_{i}^{\parallel}(n; 0) \cdot \mu_{i}^{\parallel}(m; 0) \rangle + \sum_{n} \sum_{m} \langle \mu_{i}^{\perp}(n; 0) \cdot \mu_{i}^{\perp}(m; 0) \rangle}$$
(2)

In eq 2, the first term represents the averaged relaxation of the chain end-to-end dipole and occurs on the time scale of polymer flow, and the second term represents the averaged relaxation of segmental dipole vectors on the time scale of the dynamic glass transition. Cross-terms between the polarization of dipoles within a single chain have been experimentally shown to be negligible due to the low dipole interaction energies relative to the thermal motion of the segments.⁴⁹ As for the local correlation function $C(n,t;m) = \langle \mathbf{u}(n;0) \cdot \mathbf{u}(m;t) \rangle /$ $\langle \mathbf{u}^2 \rangle$, cross-correlations among the dynamics and orientations of bond vectors $\mathbf{u}(t)$ in a neighboring chain (as opposed to polarization cross-correlations of dipoles) may not vanish due to constraints on chain motion such as chain entanglements or phase separation in block copolymer systems. Often, these orientational correlations are considered within the Kirkwood-Fröhlich correlation factor g, which is contained within the $\Delta \varepsilon$ term in eq 1. 50,51 This will be discussed further in the Dynamic Evidence of Reduced Chain Stretching section with respect to eq 3 for the 18k(12k-3k')₂ polymer. For now, all dipole motion and orientations are assumed to be incoherent, where g is unity. Further details concerning the analysis of the dielectric spectra are discussed in Part B of the Supporting Information.

Figure 2a-c displays the imaginary part of the complex dielectric function for the PSPI2 polymers at three representative temperatures. The high-frequency α -relaxation is observed at the lowest temperature, while the chain relaxation is observed at low frequencies for all temperatures. At the highest temperature, an increase in the dielectric loss spectra is observed toward low frequencies, which scales as ε'' $\sim f^{-1}$. This contribution is due to dc ionic conductivity arising from trace impurities remaining after synthesis. 52,53 The spectral shape of the chain and α -relaxations for all miktoarm star copolymers (except the 18k(12k-3k')₂ polymer) are revealed in analysis of the master curves, which are produced by shifting the ε'' spectra from 240 to 330 K by the temperature-dependent shift factors aT, which are found in Figure S7. These master curves confirm that the PI chain and α -relaxations are well separated in the time domain (cf. eq 2) and the spectral shapes of each relaxation are constant with temperature.⁵⁴ The master curve spectra in Figure S8 were fit for each polymer using two empirical Havriliak-Negami functions to reveal the spectral shapes of individual relaxations at each temperature, as detailed in Part B of the Supporting Information. For all of the polymers studied, the temperaturedependent frequency of maximum loss ($\omega_{\alpha, \max} = 2\pi f_{\alpha, \max}$) and the spectral shapes of the α -relaxation are displayed in Figure S12. The similarities in α -relaxation rates and spectral shapes among all of the polymers suggest that all PI segments within a block experience comparable local friction within the phaseseparated domains. 55 Therefore, the miktoarm architectures in this study do not affect molecular motion associated with the

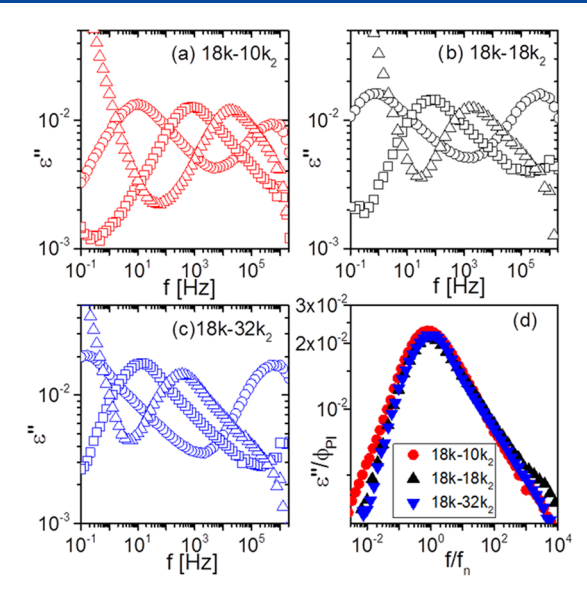


Figure 2. Dielectric loss spectra at various temperatures (circles: 260 K, squares: 300 K, triangles: 360 K) for PSPI₂ polymers (a–c). Data in (a) are reproduced from ref 16 with permission. In (d), the spectral shapes of chain relaxation spectra are presented by normalizing ε'' by PI volume fraction ($\phi_{\rm Pl}$) and frequency by the frequency of maximum loss ($f_{\rm n}$) to facilitate comparison. The error bars are smaller than the sizes of the symbols, unless specified otherwise.

length scales of the PI segments and, therefore, do not significantly affect the dynamic glass transition of the PI blocks. 56-58

In Figure 2d, the spectral shapes of the dielectric chain relaxations of the PSPI₂ polymers are normalized by PI volume fraction $(\phi_{\rm PI})$ and the frequency of maximum loss $(f_{\rm p})$. The shapes and intensities of these processes are very similar, even with increasing molecular weight and differences in morphologies among these polymers. This suggests that similar normal modes are contributing to the dielectric chain relaxation for these polymers. 59 On the other hand, the spectral shapes of the chain relaxations for the four-arm miktoarm copolymers (PS₂PI₂) vary drastically among the samples, as shown in Figure S14. These changes in PI chain relaxation spectral shapes for the PS₂PI₂ polymers are qualitatively similar to that observed for linear diblocks across different morphologies, as displayed in Figure S15. The trend in PI chain relaxation shape for different morphologies can be understood as follows. As constraints on chain motion are increased due to changes in morphology, the relaxation intensities associated with the relaxations decrease relative to the α -relaxation and span a wide frequency range, leading to "broadening" of the chain relaxation spectra. 60,61 According to the literature, an increase in spectral broadening results from a significantly slowed terminal chain relaxation. This slowing down of the terminal chain relaxation increases as the morphology changes from a continuous PI domain → lamellar → PI cylinders → PI spheres. 41 Spectral broadening is associated with increased orientational anisotropy of chain conformations and dynamic anisotropy along the chain contour with respect to the normal vector from the domain interface, as well as increased thermodynamic constraints. 41,62,63 In this context, the thermodynamic, or "osmotic", constraints are expressed as the requirement to maintain a constant segment density within the domain, and as this effect increases, there is a decrease in the available chain configurations (i.e., decrease in entropy).⁴⁹

Within the framework of the monodisperse homopolymer Gaussian chain model, the coarse-grain segments take on random configurations in all directions. On the other hand, for the Gaussian chain in phase-separated block copolymers, there is an increased segmental stretching required to maintain a constant density within the domain corresponding to a decrease in the number of available configurations.⁶⁴ In the strong segregation limit, the area per molecule within the interface is directly proportional to the free energy of mixing required to maintain the interface and is inversely related to the stretching energy that is imposed by elastic forces on the junction points. These two contributions constitute the total free energy that drives phase separation.⁶⁴ It has been determined that the area per molecule within the interface increases for the asymmetric miktoarm copolymer (A,B,,,, where $n \neq m$) compared to that for the symmetric miktoarm $(n \neq m)$ and linear diblocks. 40,65,66 Consequently, the asymmetric PSPI2 architecture has lower stretching energies compared to the symmetric architectures that display similar morphologies. Therefore, the differences in the osmotic constraint on PI chain motion that is required to maintain constant segment density among differing domain geometries are reduced for the PSPI, polymers. The reduced osmotic constraint then causes a decrease in the orientational anisotropy of chains with respect to the interface resulting in similar dielectric normal mode spectral shapes in Figure 2d for the three PSPI₂ polymers. A schematic of this effect is displayed in Figure 4b.

Dynamics and Structure of the PS(PI-PS')₂ Miktoarm Architecture (BDS and SAXS). We now turn our attention to the dynamics and structure of the PS(PI-PS')2 system. Master curves of the dielectric spectra of the 18k(12k-3k')₂ copolymer reveal that the frequency-temperature superposition does not hold as it does for all of the other miktoarm star copolymers in this study. Therefore, data for the 18k(12k-3k')₂ copolymer are presented at each individual temperature in Figure 3 with the low-frequency conductivity contribution subtracted from the spectra. Additional details regarding the fits to the dielectric spectra at each temperature for the 18k(12k-3k')₂ copolymer are found in Part B of the Supporting Information. In Figure 3a, a slow dielectric relaxation is observed at the selected temperatures for the 18k(12k-3k')₂ copolymer. In block copolymer systems where both ends of the PI chain without dipole inversion are tethered to the glassy PS interface, it is expected that no chain relaxation would be observed. 63,67 There are two possible mechanisms giving rise to the observed dielectric PI chain relaxation for the $18k(12k-3k')_2$ copolymer: (1) fluctuations of the two PI chain ends that share the junction point with the PS block or (2) fluctuations at the PI chain ends connected to the lowmolecular-weight PS' blocks, which has been described elsewhere as A' block "pull-out". 14,31,44

To verify whether the second mechanism of A' pull-out is plausible for the system reported here, the scattering invariance (Q) was determined, which provides the degree of electron density contrast across the interphase (see Table S1 for values of Q).⁶⁸ When there are only two phase-separated domains, the invariance is defined as $Q = \phi(1 - \phi)\langle\eta^2\rangle$, where ϕ is the volume fraction of either block and η is the difference in the electron density between the two phases.⁶⁹ The $18k(12k-3k')_2$ copolymer and the $18k-10k_2$ copolymer have nearly the same Q values $(1.7 \times 10^{-5} \text{ and } 1.6 \times 10^{-5} \text{ au/Å}^3$, respectively), which suggest a similar contrast in electron density between

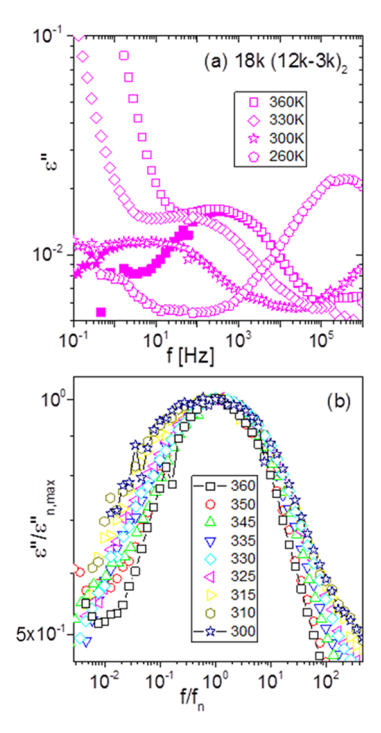


Figure 3. Dielectric loss at various temperatures as indicated for $18k(12k-3k')_2$ (open symbols) and modified dielectric loss spectra obtained by subtracting the ionic conductivity contribution at low frequencies (closed symbols) (a). In addition, the chain relaxations have been normalized by peak intensity and frequency to show a narrowing of the shape with increasing temperature (b). Error bars are smaller than the sizes of the symbols, unless specified otherwise.

the phases for the two polymers. Additionally, higher values of $I(q)q^4$ at long q (termed the Porod plot found in Figure S6) are associated with decreased thickness of the interface between scattering domains.⁷⁰ The ratio of $I(q)q^4/Q$ as $q \rightarrow$ ∞ gives a relative estimate of the geometric surface-area-tovolume ratio of the domains. ⁷⁰ The 18k(12k-3k')₂ copolymer and the $18k-10k_2$ copolymer have the lowest $I(q)q^4/Q$ values as $q \to \infty$ compared to the other polymers in this study. This indicates relatively sharp changes from PI to PS domains for the $18k(12k-3k')_2$ and the $18k-10k_2$ copolymers with a relatively narrow domain boundary thicknesses and suggests that for the $18k(12k-3k')_2$ polymer the short PS' block remains segregated from the PI domain and is embedded within the PS domain at room temperature. Therefore, we conclude that no "pull-out" occurs for the 18k(12k-3k')2 copolymer at the temperature of the SAXS measurement.

Next, to address a possible PS' pull-out at other temperatures, we note the similarity in the temperature dependence of $\omega_{\alpha,\max}$ among all of the block copolymers and the similar distributions of the relaxation times as inferred from the similar α -relaxation shapes in Figure S12. As stated in the Dynamics for Symmetric PS2PI2 and Asymmetric PSPI2 Architectures section, this similarity suggests that the local friction of the PI segments is comparable across all of the miktoarm copolymers investigated here. Additionally, the low-molecular-weight PS' block is estimated to have a $T_{\rm g} > 350~{\rm K}.^{71}$ As can be observed from Figure 3a, the PI chain relaxation for the $18{\rm k}(12{\rm k}-3{\rm k}')_2$ copolymer is measured starting at 260 K. At this temperature, the PS' chains are effectively frozen within the cylindrical PS domains. In a study by Alig et al., it was shown that in the linear triblock copolymer PS-PI-PS (with $M_{\rm wps,m} \sim 20~{\rm kg/}$

mol), the PI chain relaxation is nearly indiscernible below the $T_{\rm g}$ of the PS block due to both of the PI chain ends being immobile at the interface with the glassy PS domains. While some fluctuations of segments at the interface are expected, the length scale of these fluctuations has been determined to be ~8 monomeric units, which is less than half of the degree of polymerization of the PS' blocks. Therefore, we argue that any interphase fluctuations of the PS' segments would not significantly contribute dynamics of the PI chain ends in the $18k(12k-3k')_2$ copolymer such that the PI chain relaxation becomes active by dielectric perturbation and that the PS' block does not migrate into the PI domain at the measured temperatures and time scales.

To consider mechanism 1, we return to the SAXS profiles of the polymers with asymmetric PSPI₂ and PS(PI-PS')₂ architectures and consider the lower stretching energy of the PSPI₂ polymers in comparison with symmetric architectures, as described earlier. As determined from the SAXS analysis in the Microstructural Characterization by Small-Angle X-ray Scattering (SAXS) section, the PI chains terminated by the short PS' block in the 18k(12k-3k')₂ copolymer are stretched within the PI domain compared to those in the 18k-10k2 system. In PS-PI-PS linear triblock systems, PI chains that span the PI domain and are anchored at the interface with the PS block impart an elastic force on the junction point. 41 In the PS(PI-PS')₂ polymer architecture, however, the elastic force of the two PI chains is distributed to a single PS chain at one end and individually to two separate PS' chains at the other end. For this molecular depiction of the PS(PI-PS')2 architecture, the elastic force experienced by the PS junction imparted by the two stretched PI chains would be greater than that imposed on a single PS' junction at the other end of the PI block, as illustrated in Figure 4c. Therefore, with the PS' block determined to be immobile at experimental temperatures and time scales, and the argument for the stretching energy of two PI chains dissipated by the junction with a single PI chain, we suggest that the dynamical origin of the PI chain relaxation in the $PS(PI-PS')_2$ polymer is in the fluctuations of the PI chain ends at the PS junction point, as depicted in Figure 4c.

In Figure 3b, the slow relaxation observed from 300 K < T <360 K for the $18k(12k-3k')_2$ copolymer is normalized by the peak frequency and maximum value of the dielectric loss. This representation reveals that this relaxation narrows with increasing temperature. A narrower distribution of chain relaxation times with increasing temperature presumably corresponds to an evolution toward more homogeneous chain conformations. Additionally, the frequency of maximum loss $(\omega_{\rm p})$ of this slow relaxation is shown in Figure S13 to have an Arrhenius-like temperature dependence, which is in contrast to the temperature dependence for ω_{n} in linear diblock copolymers and all of the other miktoarm copolymers in this study which follow the Vogel-Fulcher-Tammann (VFT) equation. The VFT and Arrhenius fitting parameters for the relaxation rate data can be found in Table S3 of the Supporting Information, Part B. The Arrhenius-like temperature dependence for the slow chain relaxation is not characteristic for block copolymer chain relaxations. It has been shown that a decrease in conformational entropy (S_c) for glass formers results in a reduction in cooperative motion.⁷³ Thus, we conjecture that there is a reduction in the cooperativity associated with the PI chain dynamics for the $18k(12k-3k')_2$ system compared to that of the other polymers. The single thermal activation at experimental temperatures for chain dynamics in the 18k-

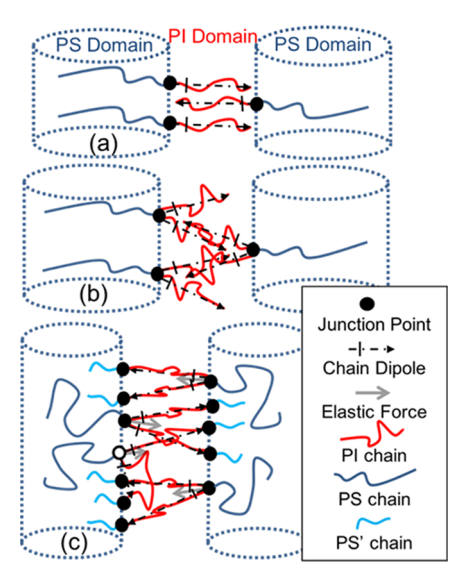


Figure 4. Schematic illustration showing chain stretching in phase-separated linear PS-b-PI diblock copolymer (a), PSPI₂ miktoarm copolymer (b), and PS(PI-PS')₂ miktoarm copolymer (c). PS cylinder morphology is chosen for simplicity. The image depicts typical chain stretching normal to the interface for the PS-b-PI polymer, which we predict to be similar to that found in the PS₂PI₂ systems. The PSPI₂ system is shown to have decreased orientational anisotropy and reduced chain stretching. The PS(PI-PS')₂ is depicted as having PI chains spanning across the PI domain as bridges. The one PS(PI-PS')₂ polymer with an unfilled junction point symbol displays the PI chain bending back to form a loop. A relative increase in elastic force is depicted at the junction of the PS and PI chains in the PS(PI-PS')₂ polymer compared to that of other PS/PI junction points as discussed in the main text.

 $(12k-3k')_2$ copolymer is, therefore, likely due to a decrease in S_c that is balanced with the relative increase in the elastic force on the junction point between the two PI chains and the PS block compared to each individual PS-PI' junction. The decrease in topological degrees of freedom of PI segments (*i.e.*, decreased S_c) is also in accordance with reductions in cooperative motions in terms of the requirement to maintain a uniform segment density (*i.e.*, osmotic constraint). With this perspective, we conclude that the dynamics of the PI chain measured by BDS in the $18k(12k-3k')_2$ copolymer is activated by fluctuations at the PS-PI₂ junction with an activation energy of 28 kJ/mol as calculated from the Arrhenius fit in Figure S13.

Dynamic Evidence of Reduced Chain Stretching. The dielectric strength of the chain relaxation $\Delta \varepsilon_{\rm n}$, which is analogous to $\Delta \varepsilon$ in eq 1 for the summed parallel dipole moment relaxation in eq 2, is displayed in Figure 5 for all of the miktoarm star copolymers. These $\Delta \varepsilon_{\rm n}$ values are normalized by absolute temperature (T) and $\phi_{\rm PI}$. For PI homopolymers, this normalized $\Delta \varepsilon_{\rm n}$ is constant with temperature above the critical molecular weight ($M_{\rm c} \sim 5000$ g/mol) and follows the dynamical description of the average chain relaxation by Gaussian statistics. Assuming monodisperse chains, the equation for dielectric strength of the chain relaxation is

$$\Delta \varepsilon_{\rm n} = \frac{4\pi N_{\rm a} \mu_{\parallel}^2}{3k_{\rm b} T M_{\rm w,PI}} F g \phi_{\rm PI} \langle R^2 \rangle \tag{3}$$

where N_a is Avogadro's number, μ_{\parallel} is the magnitude of the parallel portion of the monomeric dipole moment, k_b is

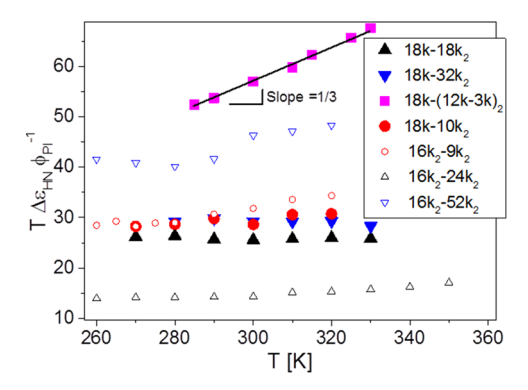


Figure 5. Normalized dielectric relaxation strength of the PI normal mode in miktoarm copolymers *versus* temperature. The solid line is a linear fit to the $18k(12k-3k')_2$ data. The strengths are multiplied by the PI volume fraction and temperature to represent the characteristic ratio, $\langle R^2 \rangle / M_{\text{w,PI}}$, of the PI chains, as described by eq 3. Error bars are smaller than the sizes of the symbols, unless specified otherwise.

Boltzmann's constant, $M_{w,PI}$ is the molecular weight of the PI arm, F is the Onsager factor that corrects for nonzero local electric field fluctuations and is assumed to be unity for all type-A polymers,⁵³ g is the Kirkwood-Fröhlich correlation factor that considers cross-correlations in the local correlation function (as briefly mentioned in the Dynamics for Symmetric PS2PI2 and Asymmetric PSPI2 Architectures section), and ϕ_{PI} is the volume fraction of PI. The $T\Delta\varepsilon_{\rm n}\phi_{\rm PI}^{-1}$ in Figure 5 are nearly temperature-independent for all PSPI2 and PS2PI2 polymers. However, with changes in PI molecular weight for the PSPI₂ polymers, the values of $T\Delta\varepsilon_{HN}\phi_{PI}^{-1}$ are constant but vary among the PS2PI2 polymers. The variations in $T\Delta\varepsilon_{\rm HN}\phi_{\rm Pl}^{-1}$ among the PS₂PI₂ samples in Figure 5 can be explained through another parameter that characterizes local constraints on chain conformations, the characteristic ratio $(C_{\infty} \sim \langle R^2 \rangle / M_{\text{w,PI}})$, which for PI homopolymer is 4.8). Assuming g = 1 for the PSPI₂ and PS₂PI₂ polymers, rearranging eq 3 shows that $T\Delta\varepsilon_n\phi_{\rm PI}^{-1}\sim \langle R^2\rangle/M_{\rm w,PI}$. The increase in PI molecular weight from the 16k2-9k2 copolymer to the 16k2-24k₂ copolymer brings about an increase in interfacial energy due to the change from spherical PI domains to lamellar morphology, which is offset with an increase in PI stretching energy in the PI spheres due to osmotic constraints. Consistent with this change in chain stretching for PI spheres, the estimate of the characteristic ratio, $C_{\infty} = \langle R^2 \rangle / N \mathbf{u}^2 \sim \langle R^2 \rangle / M_{\text{w,PI}}$, where N is the number of \mathbf{u} bond vectors of PI, is decreased for the $16k_2-24k_2$ copolymer compared to that for $16k_2-9k_2$. Conversely, the similar values of $T\Delta\varepsilon_{\rm n}\phi_{\rm PI}^{-1}\sim C_{\infty}$ for the PSPI₂ polymers suggest that the relative constraints on the PI chain segment to stretch away from the interface are relatively constant among differing morphologies for this architecture. This further indicates that the effects of morphology on chain conformation are reduced for the PSPI2 molecular architecture as compared to those for the PS2PI2 polymers.

The $T\Delta\varepsilon_{\rm HN}\phi_{\rm Pl}^{-1}$ data for $18k(12k-3k')_2$ in Figure 5, on the other hand, is greater by a factor of ~ 2 at low temperature ($\sim 285~{\rm K}$) and increases with increasing temperature. This result can be understood based on arguments made by Watanabe and co-workers on the effects of loops and bridges in PS-PI-PS triblock copolymers. These studies probed PS-PI-PS polymers with symmetric dipole inversion of the PI midblock, which allowed for a dielectrically observable chain relaxation even without any effectively free PI chain ends. 41,67

They showed that the $\Delta \varepsilon_{\rm p}$ for PS-PI-PS with dipole inversion is greater by a factor of 1.5 compared to that for the linear diblock, which has one free chain end. 41,59 This was suggested to occur because of cross-correlations in the local correlation function associated with PI chains that form knotted loops or bridges in the PS-PI-PS triblock spanning between PS domains, and, as these correlations increase and approach the case where all of the chains are knotted chains, the increase factor approaches 2.5 compared to that of the linear diblock. 59,74 In the PS(PI-PS')2 polymer in the current study, there is no dipole inversion within a single PI arm. However, we may consider the two individual chains of the PI block that are linked at the junction point with the PS block as a single probe chain with a dipole inversion at the domain interface. With this consideration, the junction point can be described as a knotted loop in a PI chain with dipole inversion at the central point between the two PI-PS' junctions in the context of the model described by Watanabe and coworkers. 59,61,74 With the relatively larger elastic force at the PS interface from the two PI chains, as described in the Dynamics and Structure of the PS(PI-PS')2 Miktoarm Architecture (BDS and SAXS) section, the motion of the PI chain between the two PS' blocks can be viewed analogously as a knotted loop. In addition to increased PI arm stiffness due to chain stretching across the interface (i.e., increased $\langle R^2 \rangle$ / $M_{\rm w.PI}$), this higher normalized dielectric relaxation strength of the PS(PI-PS')₂ polymer at low temperatures is then qualitatively ascribed to the enhanced orientational polarization of PI chains arising from knotted loops. Next, these dynamics will be discussed in terms of correlations of subchain motion to explain the empirical temperature dependence with a slope of 1/3, which in Figure 5 for the $18k(12k-3k')_2$ polymer.

In Figure 5, the normalized dielectric relaxation strength of the PI chain for the PS(PI-PS')2 polymer increases with temperature with a slope of 1/3. This linear increase has origins either in an increase in the average size of the PI chain end-to-end dipole at higher temperatures (i.e., an increase in $\langle R^2 \rangle$ corresponding to an increase in chain stiffness) or in an increase in cross-correlations of bond vector motion, $\mathbf{u}(t)$, mentioned in the Dynamics for Symmetric PS2PI2 and Asymmetric PSPI2 Architectures section, with increasing temperature. First, in conjunction with the above discussion that indicates that no pull-out occurs for the $18k(12k-3k')_2$ polymer, we posit that it is unlikely that $\langle R^2 \rangle / M_{\rm w,PI}$ would increase at $T < T_{\rm g}$ of the PS and PS' blocks. Also, Figure 3b shows that the distribution in chain relaxation times decreases with increasing temperature, which is contrary to an increased chain stretching with increasing temperature. Therefore, we explore the possibility of increased correlations in subchain motion through nonzero cross-terms among $\mathbf{u}(t)$ in the local correlation function C(n,t;m) from eq 1 as parameterized by g

The Kirkwood correlation factor is defined as $g=1+\langle\cos\theta_{i,j}\rangle$, where $\theta_{i,j}$ is the angle of the dipole moment vector of the "ith" chain with respect to the "jth" nearest-neighbor chain dipole vector. For g=1, there are no correlations in dipole orientation. For g>1, the correlations in dipole orientation are more parallel. Finally, 0 < g < 1 indicates that dipoles are oriented more antiparallel. Using the Doi and Edwards tube model, it was determined that g=4/5 for entangled homopolymer chains by considering the equilibration of subchain tension during relaxation, which places a nonzero

force far from the chain ends. 77,78 Additionally, Watanabe showed that for the coherent motion of polymer subchains (i.e., cross-correlations of subchains at long times), the decrease in g for entangled chains is due to a decrease in the initial orientational anisotropy of subchains during the contour length fluctuation mechanism (also termed dynamic tube dilation).61 In other words, there is enhanced motion near the chain ends compared to that of interior subchains, which are confined by entanglements increasing isotropy in chain orientation during relaxation.⁷⁹ Furthermore, in lamellae forming PS-b-PI diblock systems, there is a direct correlation between an antiparallel chain orientation across the domains and the chain end-to-end distances as the chains stretch away from the interface. 80,81 In the PS(PI-PS')₂ polymer, we assert that PI chains are statically stretched between the PS domains. This decreases the orientational anisotropy at low temperatures compared to the PSPI₂ polymers. As the temperature increases, the elastic forces on the junction points required to maintain the interface decrease, which releases subchain tension during relaxation toward equilibrium. This mechanism subsequently enhances the contributions of knot-like dynamics and corresponds to a decreased fraction of antiparallel chain orientations in the PS(PI-PS')2 polymer as the temperature increases.⁸² Then, as the subchain tension is reduced with increasing temperature, there is a shift toward a more homogeneous distribution in chain relaxation rates with increasing temperature, observed in Figure 3b. This coincides with a reduction in g analogous to entangled homopolymer chains due to the nonzero subchain tension. Through these arguments, a positive slope in the temperature dependence of $T\Delta\varepsilon_{\rm n}\phi_{\rm PI}^{-1}$ in Figure 5 for the PS(PI-PS')₂ polymer is rationalized through correlations in chain relaxation dynamics, as parameterized by g = 1/3. For more details regarding the connection of g to the Gaussian chain model, see Part C in the Supporting Information.

Finally, Figure 6 displays the molecular weight dependence of $\tau_{\rm n}$ at 320 K for all of the miktoarm systems, along with data from the literature. The prediction by Doi and Edwards for the relaxation times of normal modes of entangled flexible homopolymers is

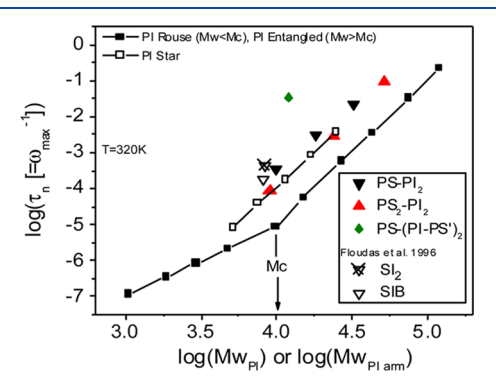


Figure 6. Mean PI chain relaxation times (τ_n) at 320 K plotted *versus* PI arm molecular weight $(M_{w_{\text{PI},\text{am}}})$ for all miktoarm copolymers studied with data for linear and star PI homopolymers from the literature. ^{49,53,75,83} Additional PSPI₂ time scales are included from the literature for "SI₂", which is analogous to PSPI₂, and "SIB", which has one polyisoprene block replaced by polybutadiene. ³⁶ Error bars are smaller than the sizes of the symbols, unless specified otherwise.

$$\tau_{\rm p} = \frac{\varsigma N^3 b^4}{\pi^2 k_{\rm b} T a^2 p^2} \tag{4}$$

where ς accounts for local friction, N is the number of segments in the polymer chain, b is the segment length, a is the Rouse tube diameter (which accounts for entanglements of chains), T is the absolute temperature, $k_{\rm b}$ is the Boltzmann constant, and p is an integer corresponding to the eigenvalue of the chain relaxation mode. Figure 6 shows data of entangled homopolymer PI (closed squares), which follow the experimental power law of $\tau_{\rm n} \sim M_{\rm w,PI}^{3.7}$, which deviates slightly from the prediction of eq 4. This power law holds for tethered PI such as in phase-separated PS-b-PI linear diblock copolymers and PI star homopolymers (open squares), but with a 4-fold increase compared to free chains $(4\tau_n =$ $au_{\rm n,tethered}$). Ror the PS₂PI₂ polymers (red up-triangles), these predictions hold quantitatively. We note that because the spectral shapes of the chain relaxations for the PS₂PI₂ polymers in this study are quite different, it is not evident that the same normal modes are probed by BDS, and the constraints on chain motion are likely dissimilar among differing morphologies similar to linear PS-PI systems. 49 On the other hand, the spectral shapes of the PI chain relaxation in the PSPI₂ systems are morphology and molecular-weight-independent (cf. Figure 2d). In Figure 6, the values of τ_n for PI in the PSPI₂ systems (black down-triangles) are slightly increased at the same molecular weight compared with the τ_n for systems with symmetric chain topologies. Also, there is a slightly reduced molecular weight dependence $\tau_{\rm n,PSPI2} \sim M_{\rm w,PI}^{3.5}$ for the PSPI₂ systems. To the best of our knowledge, only one other study has reported the PI chain dielectric relaxation times of a PSPI₂ miktoarm star copolymer.³⁶ The chain relaxation time for the PSPI₂ polymer in the work by Floudas et al. at 320 K (open down-triangle) is also plotted against the PI arm molecular weight in Figure 6 and agrees with the $M_{\rm w}$ dependence for our PSPI₂ polymers. Additionally, the spectral shape of the chain relaxation for their PSPI₂ polymer (shown in Figure S16) is observed to be similar to those in our measurements. From eq 4 and our arguments regarding chain stretching and area per molecule at the interface, it is likely that the marginally slower chain relaxation times for the PSPI2 polymers at a given molecular weight are most likely due to some combination of an average decrease in a and an increase in c, which follows results from models that predict that the increased friction and decreased confining tube diameter correspond to decreased stretching, as described here for the PSPI₂ polymers.^{88,89} Therefore, due to decreased osmotic constraints on the chain relaxations, chain stretching is alleviated for the PSPI2 polymers compared to the symmetric architectures of the PS_2PI_2 miktoarm and linear diblock systems. $^{77,90-92}$ On the other hand, the \sim 3 order of magnitude increase in τ_n for the $18k(12k-3k')_2$ polymer is consistent with highly stretched but tethered PI chains and corresponds to a significant increase in the tube diameter restricting the chain relaxation to much longer times. 93,94

In summary, the architecturally asymmetric miktoarm star copolymer systems (PSPI₂) feature distributions in chain relaxation times and dielectric relaxation strengths that are not dependent on molecular weight or morphology, in stark contrast to the effects of morphological confinement observed for symmetric diblock systems (PS-b-PI or PS₂PI₂). This disparity is argued to be due to reduced chain stretching for the asymmetric systems. The segmental relaxations for all PI

chains are observed to be comparable for all architectures and morphologies considered in this study. Finally, to strengthen the argument regarding chain stretching and dynamics, the PI chain relaxation was measured for the PS(PI-PS')₂ polymer. This chain relaxation is observed even with the two PI chains linked at both ends with the PS or PS' blocks and has an increased dielectric relaxation strength compared to other PI systems with an additional temperature dependence, which we attribute to increased chain stretching and subchain crosscorrelations with temperature. 40,95 These results are useful in understanding the role of architectural asymmetry in miktoarm star polymers, particularly for the PS(PI-PS')₂ architecture, which has been shown to be important for tough thermoplastic elastomers due to enhanced chain bridging as discussed here in terms of the dynamics of knotted loops and bridges of PI chains.3

CONCLUSIONS

Based on the results and arguments presented above, we conclude that in phase-separated miktoarm star copolymer systems, topological asymmetry in the number of arms in each block gives rise to more uniform chain motion among selfassembled phases compared to block copolymers with symmetric molecular architecture. This was determined through investigation of the spectral shapes and dielectric strengths of the PI chain relaxations among different molecular weights for three PSPI₂ polymers, in contrast to the varied dynamics observed among the symmetric PS₂PI₂ polymers, which more closely resemble that of classic linear PS-b-PI systems. Additionally, the chain relaxation times at 320 K for various PI molecular weights in the PSPI, polymers are slightly increased compared to the τ_n for other tethered PI systems. This reveals that the architectural imbalance in the number of arms per block plays a role in the dynamics of rubbery polymer chains. Furthermore, a dielectric chain relaxation is observed for the PS(PI-PS')₂ miktoarm star copolymer where both PI chain ends are embedded in the glassy PS' domain. Compared to the practically undetectable PI dielectric chain relaxation in PS-PI-PS linear triblock copolymers, the dramatically slower PI chain dynamics are observed to exhibit a narrower relaxation time distribution and have an increased, temperature-dependent $\Delta \varepsilon_{\rm n}$ compared to the other PI systems. We argue that these chain dynamics result from an elastic force imbalance at the PI chain ends due to the trifunctional junction point of the PS block and two PI chains and from contributions to the dielectric spectrum due to crosscorrelations in chain motion as parameterized through the Kirkwood–Fröhlich factor (g). These results were discussed in terms of the counterbalance among contributions to the free energy of phase separation from chain stretching and interface formation with supporting data from SAXS. We demonstrate that subtle modifications to molecular architecture can have a substantial impact on the internal constraints that govern polymer chain dynamics, which ultimately determines macroscopic physicochemical properties in polymeric systems.

ASSOCIATED CONTENT

Supporting Information

The Supporting Information is available free of charge at https://pubs.acs.org/doi/10.1021/acs.macromol.0c01858.

Additional information regarding analysis of the microstructure by TEM, SAXS profiles, and calculation of the scattering invariance (Part A); analysis of the dielectric data, relaxation rates, and comparison of chain relaxation spectral shapes to literature data (Part B); and a summary connecting the Kirkwood correlation factor with the Gaussian chain (Part C) are provided (PDF)

AUTHOR INFORMATION

Corresponding Author

Joshua Sangoro — Department of Chemical and Biomolecular Engineering, University of Tennessee, Knoxville, Tennessee 37996, United States; orcid.org/0000-0002-5483-9528; Email: jsangoro@utk.edu

Authors

Thomas Kinsey — Department of Chemical and Biomolecular Engineering, University of Tennessee, Knoxville, Tennessee 37996, United States; orcid.org/0000-0002-1107-4449

Emmanuel Urandu Mapesa — Department of Chemical and Biomolecular Engineering, University of Tennessee, Knoxville, Tennessee 37996, United States; orcid.org/0000-0002-2206-0990

Weiyu Wang — Center for Nanophase Materials Science, Oak Ridge National Laboratory, Oak Ridge, Tennessee 37831, United States; © orcid.org/0000-0002-2914-1638

Kunlun Hong — Department of Chemical and Biomolecular Engineering, University of Tennessee, Knoxville, Tennessee 37996, United States; Center for Nanophase Materials Science, Oak Ridge National Laboratory, Oak Ridge, Tennessee 37831, United States; orcid.org/0000-0002-2852-5111

Jimmy Mays – Department of Chemistry, University of Tennessee, Knoxville, Tennessee 37996, United States

S. Michael Kilbey, II — Department of Chemical and Biomolecular Engineering, University of Tennessee, Knoxville, Tennessee 37996, United States; Department of Chemistry, University of Tennessee, Knoxville, Tennessee 37996, United States; Occid.org/0000-0002-9431-1138

Complete contact information is available at: https://pubs.acs.org/10.1021/acs.macromol.0c01858

Notes

The authors declare no competing financial interest.

ACKNOWLEDGMENTS

Financial support for contributions made by T.K., E.U.M., and J.S. was from the National Science Foundation (NSF), Division of Materials Research, Polymers Program through DMR-1508394. S.M.K. acknowledges financial support from the National Science Foundation through DMR-1905487. Small-angle X-ray scattering measurements were made at Duke University Shared Materials Instrumentation Facility (SMIF), a member of the North Carolina Research Triangle Nanotechnology Network (RTNN), with help from Justin Gladman. The SMIF is supported by the NSF (Grant ECSS-1542015) as part of the National Nanotechnology Coordinated Infrastructure (NNCI). Transmission electron microscopy images were obtained through the Joint Institute for Advanced Materials at the University of Tennessee, Knoxville's Cherokee Farm campus, with help from John Dunlap. The materials used in this study were synthesized at the Center for Nanophase Materials Sciences, which is a DOE Office of Science User

Facility. W.W. and J.M. acknowledge support from DOE, Basic Energy Sciences, Materials Science and Engineering Division.

REFERENCES

- (1) Burns, A. B.; Register, R. A. Mechanical Properties of Star Block Polymer Thermoplastic Elastomers with Glassy and Crystalline End Blocks. *Macromolecules* **2016**, *49*, 9521–9530.
- (2) Bates, F. S.; Bates, C. M. 50th Anniversary Perspective: Block Polymers—Pure Potential. *Macromolecules* **2017**, *50*, 3–22.
- (3) Wijayasekara, D. B.; Huang, T.; Richardson, J. M.; Knauss, D. M.; Bailey, T. S. The Role of Architecture in the Melt-State Self-Assembly of (Polystyrene)_{star}-b-(Polyisoprene)_{linear}-b-(Polystyrene)_{star}-b-(Pom-Pom Triblock Copolymers. *Macromolecules* **2016**, *49*, 595–608.
- (4) Burns, A. B.; Register, R. A. Strategies for the Synthesis of Well-Defined Star Polymers by Anionic Polymerization with Chlorosilane Coupling and Preservation of the Star Architecture during Catalytic Hydrogenation. *Macromolecules* **2016**, *49*, 2063–2070.
- (5) Uhrig, D.; Mays, J. W. Experimental techniques in high-vacuum anionic polymerization. *J. Polym. Sci., Part A: Polym. Chem.* **2005**, 43, 6179–6222.
- (6) Levi, A. E.; Fu, L.; Lequieu, J.; Horne, J. D.; Blankenship, J.; Mukherjee, S.; Zhang, T.; Fredrickson, G. H.; Gutekunst, W. R.; Bates, C. M. Efficient Synthesis of Asymmetric Miktoarm Star Polymers. *Macromolecules* **2020**, 53, 702–710.
- (7) Uhrig, D.; Schlegel, R.; Weidisch, R.; Mays, J. Multigraft copolymer superelastomers: Synthesis morphology, and properties. *Eur. Polym. J.* **2011**, 47, 560–568.
- (8) Feng, H.; Lu, X.; Wang, W.; Kang, N. G.; Mays, J. W. Block Copolymers: Synthesis, Self-Assembly, and Applications. *Polymers* **2017**, *9*, No. 494.
- (9) Polymeropoulos, G.; Zapsas, G.; Ntetsikas, K.; Bilalis, P.; Gnanou, Y.; Hadjichristidis, N. 50th Anniversary Perspective: Polymers with Complex Architectures. *Macromolecules* **2017**, *50*, 1253–1290.
- (10) Li, B.; Zhu, Y. L.; Lu, Z. Y. Note: Different micellization behavior of miktoarm star-like and diblock copolymers. *J. Chem. Phys.* **2012**, *137*, No. 246102.
- (11) Khanna, K.; Varshney, S.; Kakkar, A. Miktoarm star polymers: advances in synthesis, self-assembly, and applications. *Polym. Chem.* **2010**, *1*, 1171.
- (12) Shi, W.; Tateishi, Y.; Li, W.; Hawker, C. J.; Fredrickson, G. H.; Kramer, E. J. Producing Small Domain Features Using Miktoarm Block Copolymers with Large Interaction Parameters. *ACS Macro Lett.* **2015**, *4*, 1287–1292.
- (13) Matsen, M. W. Effect of Architecture on the Phase Behavior of AB-Type Block Copolymer Melts. *Macromolecules* **2012**, *45*, 2161–2165.
- (14) Lynd, N. A.; Oyerokun, F. T.; O'Donoghue, D. L.; Handlin, D. L.; Fredrickson, G. H. Design of Soft and Strong Thermoplastic Elastomers Based on Nonlinear Block Copolymer Architectures Using Self-Consistent-Field Theory. *Macromolecules* **2010**, *43*, 3479–3486.
- (15) Zhao, M.; Li, W. Laves Phases Formed in the Binary Blend of AB4 Miktoarm Star Copolymer and A-Homopolymer. *Macromolecules* **2019**, *52*, 1832–1842.
- (16) Hayashida, K.; Takano, A.; Arai, S.; Shinohara, Y.; Amemiya, Y.; Matsushita, Y. Systematic Transitions of Tiling Patterns Formed by ABC Star-Shaped Terpolymers. *Macromolecules* **2006**, *39*, 9402–9408.
- (17) Matsushita, Y.; Hayashida, K.; Dotera, T.; Takano, A. Kaleidoscopic morphologies from ABC star-shaped terpolymers. *J. Phys.: Condens. Matter* **2011**, 23, No. 284111.
- (18) Reddy, A.; Buckley, M. B.; Arora, A.; Bates, F. S.; Dorfman, K. D.; Grason, G. M. Stable Frank-Kasper phases of self-assembled, soft matter spheres. *Proc. Natl. Acad. Sci. U.S.A.* **2018**, *115*, 10233–10238.
- (19) Xie, N.; Li, W.; Qiu, F.; Shi, A.-C. σ Phase Formed in Conformationally Asymmetric AB-Type Block Copolymers. ACS Macro Lett. 2014, 3, 906–910.
- (20) Liu, Y.-X.; Delaney, K. T.; Fredrickson, G. H. Field-Theoretic Simulations of Fluctuation-Stabilized Aperiodic "Bricks-and-Mortar"

- Mesophase in Miktoarm Star Block Copolymer/Homopolymer Blends. *Macromolecules* **2017**, *50*, 6263–6272.
- (21) Bates, M. W.; Barbon, S. M.; Levi, A. E.; Lewis, R. M.; Beech, H. K.; Vonk, K. M.; Zhang, C.; Fredrickson, G. H.; Hawker, C. J.; Bates, C. M. Synthesis and Self-Assembly of ABn Miktoarm Star Polymers. ACS Macro Lett. 2020, 9, 396–403.
- (22) Shi, W.; Lynd, N. A.; Montarnal, D.; Luo, Y.; Fredrickson, G. H.; Kramer, E. J.; Ntaras, C.; Avgeropoulos, A.; Hexemer, A. Toward Strong Thermoplastic Elastomers with Asymmetric Miktoarm Block Copolymer Architectures. *Macromolecules* **2014**, *47*, 2037–2043.
- (23) Miller, K. Miktoarm Star Polymers as Functional and Responsive Materials. University of Illinois, Materials Siminar Abstract, 2015.
- (24) Hore, M. J. A. Polymers on nanoparticles: structure & dynamics. *Soft Matter* **2019**, *15*, 1120–1134.
- (25) Johnson, J. M.; Allgaier, J. B.; Wright, S. J.; Young, R. N.; et al. Linear Rheological Behaviour of Polyisoprene-Polystyrene Heterostar and Linear Diblock Copolymer Melts. *J. Chem. Soc., Faraday Trans.* 1995, 91, 2403–2409.
- (26) Erwin, A. J.; Lee, H.; Ge, S.; Zhao, S.; Korolovych, V. F.; He, H.; Matyjaszewski, K.; Sokolov, A. P.; Tsukruk, V. V. Viscoelastic properties and ion dynamics in star-shaped polymerized ionic liquids. *Eur. Polym. J.* **2018**, *109*, 326–335.
- (27) Guan, T.; Qian, S.; Guo, Y.; Cheng, F.; Zhang, W.; Chen, J. Star Brush Block Copolymer Electrolytes with High Ambient-Temperature Ionic Conductivity for Quasi-Solid-State Lithium Batteries. ACS Mater. Lett. 2019, 606—612.
- (28) Lee, D.; Jung, H. Y.; Park, M. J. Solid-State Polymer Electrolytes Based on AB3-Type Miktoarm Star Copolymers. *ACS Macro Lett.* **2018**, *7*, 1046–1050.
- (29) Xiao, Z.; Zhou, B.; Wang, J.; Zuo, C.; He, D.; Xie, X.; Xue, Z. PEO-based electrolytes blended with star polymers with precisely imprinted polymeric pseudo-crown ether cavities for alkali metal ion batteries. *J. Membr. Sci.* **2019**, *576*, 182–189.
- (30) Shi, W.; Hamilton, A. L.; Delaney, K. T.; Fredrickson, G. H.; Kramer, E. J.; Ntaras, C.; Avgeropoulos, A.; Lynd, N. A.; Demassieux, Q.; Creton, C. Aperiodic "Bricks and Mortar" Mesophase: a New Equilibrium State of Soft Matter and Application as a Stiff Thermoplastic Elastomer. *Macromolecules* **2015**, *48*, 5378–5384.
- (31) Lequieu, J.; Koeper, T.; Delaney, K. T.; Fredrickson, G. H. Extreme Deflection of Phase Boundaries and Chain Bridging in A(BA')n Miktoarm Star Polymers. *Macromolecules* **2020**, *53*, 513–522.
- (32) Bates, F. S.; Maurer, W. W.; Lipic, P. M.; Hillmyer, M. A.; Almdal, K.; Mortensen, K.; Fredrickson, G. H.; Lodge, T. P. Polymeric Bicontinuous Microemulsions. *Phys. Rev. Lett.* **1997**, 79, 849–852.
- (33) Ellison, C. J.; Meuler, A. J.; Qin, J.; Evans, C. M.; Wolf, L. M.; Bates, F. S. Bicontinuous polymeric microemulsions from polydisperse diblock copolymers. *J. Phys. Chem. B* **2009**, *113*, 3726–3737.
- (34) Hillmyer, M. A.; Maurer, W. W.; Lodge, T. P.; Bates, F. S.; Almdal, K. Model Bicontinuous Microemulsions in Ternary Homopolymer/Block Copolymer Blends. *J. Phys. Chem. B* **1999**, 103, 4814–4824.
- (35) Hebbeker, P.; Plamper, F. A.; Schneider, S. Effect of the Molecular Architecture on the Internal Complexation Behavior of Linear Copolymers and Miktoarm Star Polymers. *Macromol. Theory Simul.* **2015**, *24*, 110–116.
- (36) Floudas, G.; Hadjichristidis, N.; Iatrou, H.; Pakula, T. Microphase Separation in Model 3-Miktoarm Star Co- and Terpolymers. 2. Dynamics. *Macromolecules* **1996**, 29, 3139–3146.
- (37) Hinestrosa, J. P.; Alonzo, J.; Osa, M.; Kilbey, S. M. Solution Behavior of Polystyrene-Polyisoprene Miktoarm Block Copolymers in a Selective Solvent for Polyisoprene. *Macromolecules* **2010**, *43*, 7294–7304.
- (38) Gambino, T.; Alegría, A.; Arbe, A.; Colmenero, J.; Malicki, N.; Dronet, S.; Schnell, B.; Lohstroh, W.; Nemkovski, K. Applying Polymer Blend Dynamics Concepts to a Simplified Industrial System. A Combined Effort by Dielectric Spectroscopy and Neutron Scattering. *Macromolecules* **2018**, *51*, 6692–6706.

- (39) Mortensen, K.; Borger, A. L.; Kirkensgaard, J. J. K.; Garvey, C. J.; Almdal, K.; Dorokhin, A.; Huang, Q.; Hassager, O. Structural Studies of Three-Arm Star Block Copolymers Exposed to Extreme Stretch Suggests a Persistent Polymer Tube. *Phys. Rev. Lett.* **2018**, 120, No. 207801.
- (40) Kinsey, T.; Mapesa, E. U.; Wang, W.; Hong, K.; Mays, J.; Kilbey, S. M.; Sangoro, J. Impact of Molecular Architecture on Dynamics of Miktoarm Star Copolymers. *Macromolecules* **2018**, *51*, 5401–5408.
- (41) Matsumiya, Y.; Chen, Q.; Uno, A.; Watanabe, H.; Takano, A.; Matsuoka, K.; Matsushita, Y. Dielectric behavior of Styrene–Isoprene (SI) Diblock and SIIS Triblock Copolymers: Global Dynamics of I Blocks in Spherical and Cylindrical Domains Embedded in Glassy S Matrix. *Macromolecules* **2012**, *45*, 7050–7060.
- (42) Matsen, M. W.; Gardiner, J. M. Anomalous domain spacing difference between AB diblock and homologous A2B2 starblock copolymers. *J. Chem. Phys.* **2000**, *113*, 1673–1676.
- (43) Hamley, I.; Castelletto, V. Small-Angle Scattering of Block Copolymers. In *Soft Matter Characterization*; Borsali, R.; Pecora, R., Eds.; Springer: Dordrecht, 2008; pp 1021–1081.
- (44) Matsen, M. W. Equilibrium behavior of asymmetric ABA triblock copolymer melts. J. Chem. Phys. 2000, 113, No. 5539.
- (45) Sakurai, S.; Shirouchi, K.; Munakata, S.; Kurimura, H.; Suzuki, S.; Watanabe, J.; Oda, T.; Shimizu, N.; Tanida, K.; Yamamoto, K. Morphology Reentry with a Change in Degree of Chain Asymmetry in Neat Asymmetric Linear A1BA2 Triblock Copolymers. *Macromolecules* **2017**, *50*, 8647–8657.
- (46) Watanabe, H.; Tan, H. Dielectric Investigation of Bridge Fraction in Triblock/Diblock Mixed Lamella. *Macromolecules* **2004**, 37, 5118–5122.
- (47) Stockmayer, W. H.; Baur, M. E. Low-Frequency Electrical Response of Flexible Chain Molecules. *J. Am. Chem. Soc.* **1964**, *86*, 3485–3489.
- (48) Bahar, I.; Erman, B.; Kremer, F.; Fischer, E. W. Segmental motions of cis-polyisoprene in the bulk state: interpretation of dielectric relaxation data. *Macromolecules* **1992**, *25*, 816–825.
- (49) Yao, M. L.; Watanabe, H.; Adachi, K.; Kotaka, T. Dielectric relaxation behavior of styrene-isoprene diblock copolymers: bulk systems. *Macromolecules* **1991**, 24, 2955–2962.
- (50) Brodin, A. Segmental versus chain dynamics of linear polymers. *J. Chem. Phys.* **2008**, *128*, No. 104901.
- (51) Yamane, M.; Hirose, Y.; Adachi, K. Dielectric Normal and Segmental Modes in Undiluted Poly(butylene oxide). *Macromolecules* **2005**, 38, 9210–9215.
- (52) Kipnusu, W. K.; Elmahdy, M. M.; Mapesa, E. U.; Zhang, J.; Bohlmann, W.; Smilgies, D. M.; Papadakis, C. M.; Kremer, F. Structure and Dynamics of Asymmetric Poly(styrene-b-1,4-isoprene) Diblock Copolymer under 1D and 2D Nanoconfinement. ACS Appl. Mater. Interfaces 2015, 7, 12328–12338.
- (53) Kremer, F.; Schönhals, A. Broadband Dielectric Spectroscopy, 1st ed.; Springer: Berlin, 2003; p 729.
- (54) Jenczyk, J.; Dobies, M.; Makrocka-Rydzyk, M.; Wypych, A.; Jurga, S. The segmental and global dynamics in lamellar microphase-separated poly(styrene-b-isoprene) diblock copolymer studied by 1H NMR and dielectric spectroscopy. *Eur. Polym. J.* **2013**, *49*, 3986–3007
- (55) Yao, M. L.; Watanabe, H.; Adachi, K.; Kotaka, T. Dielectric relaxation of styrene-isoprene diblock copolymer solutions: a common solvent system. *Macromolecules* **1992**, *25*, 1699–1704.
- (56) Alig, I.; Kremer, F.; Fytas, G.; Roovers, J. Dielectric relaxation in disordered poly(isoprene-styrene) diblock copolymers near the microphase-separation transition. *Macromolecules* **1992**, *25*, 5277–5282.
- (57) Bates, F. S.; Rosedale, J. H.; Fredrickson, G. H. Fluctuation effects in a symmetric diblock copolymer near the order–disorder transition. *J. Chem. Phys.* **1990**, *92*, *6255–6270*.
- (58) Rizos, A. K.; Fytas, G.; Roovers, J. E. L. Segmental motion in poly(styrene-b-1,4-isoprene) block copolymers in the disordered state. *J. Chem. Phys.* **1992**, *97*, 6925–6932.

- (59) Watanabe, H.; Sato, T.; Osaki, K.; Matsumiya, Y.; Anastasiadis, S. H. Effects of Spatial Confinement on Dielectric Relaxations of Block Copolymers having Tail, Loop, and Bridge Conformations. *J. Soc. Rheol., Jpn.* **1999**, *27*, 173–182.
- (60) Adachi, K.; Kotaka, T. Dielectric normal mode relaxation of tethered polyisoprene chains in styrene-isoprene block copolymers. *Pure Appl. Chem.* **1997**, *69*, 125–130.
- (61) Watanabe, H. Slow Dynamics in Homopolymer Liquids. *Polym. J.* **2009**, *41*, 929–950.
- (62) Bates, F. S.; Fredrickson, G. H. Block Copolymer Thermodynamics: Theory and Experiment. *Annu. Rev. Phys. Chem.* **1990**, *41*, 525–557.
- (63) Chen, Q.; Matsumiya, Y.; Iwamoto, T.; Nishida, K.; Kanaya, T.; Watanabe, H.; Takano, A.; Matsuoka, K.; Matsushita, Y. Dielectric Behavior of Guestcis-Polyisoprene Confined in Spherical Microdomain of Triblock Copolymer. *Macromolecules* **2012**, *45*, 2809–2810
- (64) Matsen, M. W. The standard Gaussian model for block copolymer melts. *J. Phys.: Condens. Matter* **2002**, *14*, R21–R47.
- (65) Tselikas, Y.; Iatrou, H.; Hadjichristidis, N.; Liang, K. S.; Mohanty, K.; Lohse, D. J. Morphology of miktoarm star block copolymers of styrene and isoprene. *J. Chem. Phys.* **1996**, *105*, 2456.
- (66) Winey, K. I. Morphologies and Morphological Transitions in Binary Blends of Diblock Copolymer and Homopolymer. Doctoral Dissertations 1896—February 2014, University of Massachusetts Amherst, 1991.
- (67) Watanabe, H. Slow Dielectric Relaxation of a Styrene-Isoprene-Styrene Triblock Copolymer with Dipole Inversion in the Middle Block: A Challenge to a Loop/Bridge Problem. *Macromolecules* **1995**, 28, 5006–5011.
- (68) Spalla, O.; Lyonnard, S.; Testard, F. Analysis of the small-angle intensity scattered by a porous and granular medium. *J. Appl. Crystallogr.* **2003**, *36*, 338–347.
- (69) Brinker, K. L.; Lebovitz, A. H.; Torkelson, J. M.; Burghardt, W. R. Porod scattering study of coarsening in immiscible polymer blends. *J. Polym. Sci., Part B: Polym. Phys.* **2005**, *43*, 3413–3420.
- (70) Boldon, L.; Laliberte, F.; Liu, L. Review of the fundamental theories behind small angle X-ray scattering, molecular dynamics simulations, and relevant integrated application. *Nano Rev.* **2015**, *6*, No. 25661.
- (71) Claudy, P.; Letoffe, J. M.; Camberlain, Y.; Pascault, J. P. Glass transition of polystyrene versus molecular weight. *Polym. Bull.* **1983**, 9–9, 208–215.
- (72) Alig, I.; Floudas, G.; Avgeropoulos, A.; Hadjichristidis, N. Junction Point Fluctuations in Microphase Separated Polystyrene-Polyisoprene-Polystyrene Triblock Copolymer Melts. A Dielectric and Rheological Investigation. *Macromolecules* 1997, 30, 5004–5011.
- (73) Mauro, J. C.; Yue, Y.; Ellison, A. J.; Gupta, P. K.; Allan, D. C. Viscosity of glass-forming liquids. *Proc. Natl. Acad. Sci. U.S.A.* **2009**, 106, 19780–19784.
- (74) Watanabe, H. Dielectric Relaxation of Type-A Polymers in Melts and Solutions. *Macromol. Rapid Commun.* **2001**, 22, 127–175.
- (75) Elfadl, A. A.; Kahlau, R.; Herrmann, A.; Novikov, V. N.; Rössler, E. A. From Rouse to Fully Established Entanglement Dynamics: A Study of Polyisoprene by Dielectric Spectroscopy. *Macromolecules* **2010**, *43*, 3340–3351.
- (76) Tanaka, S.; Nakajima, A. Unperturbed Chain Dimensions of Stereoirregular 1,4-Polybutadiene and 1, 4-Polyisoprene. *Polym. J.* **1972**, 3, 500–506.
- (77) Doi, M.; Edwards, S. F. The Theory of Polymer Dynamics; Oxford University Press: New York, 1988.
- (78) Watanabe, H.; Matsumiya, Y.; Osaki, K.; Yao, M.-L. Dynamics of Dipole-Invertedcis-Polyisoprene Chains in a Matrix of Long, Entangling Chains. 2. Effects of Constraint Release on the Coherence of the Subchain Motion. *Macromolecules* 1998, 31, 7538–7545.
- (79) Kumar, R.; Goswami, M.; Sumpter, B. G.; Novikov, V. N.; Sokolov, A. P. Effects of backbone rigidity on the local structure and dynamics in polymer melts and glasses. *Phys. Chem. Chem. Phys.* **2013**, 15, 4604–4609.

- (80) Sethuraman, V.; Kipp, D.; Ganesan, V. Entanglements in Lamellar Phases of Diblock Copolymers. *Macromolecules* **2015**, *48*, 6321–6328.
- (81) Grason, G. The packing of soft materials: Molecular asymmetry, geometric frustration and optimal lattices in block copolymer melts. *Phys. Rep.* **2006**, 433, 1–64.
- (82) Böttcher, C. J. F. *Theory of Electric Polarisation*, 2nd ed.; Elsevier Scientific Publishing Company: Amsterdam, 1973.
- (83) Boese, D.; Kremer, F.; Fetters, L. J. Molecular dynamics in linear- and star-branched polymers of cis-polyisoprene as studied by dielectric spectroscopy. *Makromol. Chem., Rapid Commun.* **1988**, *9*, 367–371.
- (84) Boese, D.; Kremer, F.; Fetters, L. J. Molecular dynamics in linear and multiarmed star polymers of cis-polyisoprene as studied by dielectric spectroscopy. *Macromoleules* **1990**, 23, 1826–1830.
- (85) Serghei, A.; Kremer, F. Confinement-induced relaxation process in thin films of cis-polyisoprene. *Phys. Rev. Lett.* **2003**, *91*, No. 165702.
- (86) Graessley, W. W. Entangled Linear, Branched and Network Polymer Systems—Molecular Theories; Springer: Berlin, Heidelberg, 1982; Vol. 47, pp 67–117.
- (87) Graessley, W. Viscoelasticity and Diffusion in Entangled Polymer Melts; Elsevier Science Publishers, 1988.
- (88) Read, D. J. Convective constraint release with chain stretch: Solution of the Rouse-tube model in the limit of infinite tubes. *J. Rheol.* **2004**, *48*, 349–377.
- (89) Bobbili, S. V.; Milner, S. T. Chain tension reduces monomer friction in simulated polymer melts. *J. Rheol.* **2020**, *64*, 1373–1378.
- (90) Watanabe, H.; Matsumiya, Y.; Osaki, K. Tube Dilation Process in Star-Branched cis-Polyisoprenes. *J. Polym. Sci., Part B: Polym. Phys.* **2000**, *38*, 1024–1036.
- (91) Watanabe, H.; Matsumiya, Y.; van Ruymbeke, E.; Vlassopoulos, D.; Hadjichristidis, N. Viscoelastic and Dielectric Relaxation of a Cayley-Tree-Type Polyisoprene: Test of Molecular Picture of Dynamic Tube Dilation. *Macromolecules* **2008**, *41*, 6110–6124.
- (92) Matsumiya, Y.; Masubuchi, Y.; Inoue, T.; Urakawa, O.; Liu, C.-Y.; van Ruymbeke, E.; Watanabe, H. Dielectric and Viscoelastic Behavior of Star-Branched Polyisoprene: Two Coarse-Grained Length Scales in Dynamic Tube Dilation. *Macromolecules* **2014**, *47*, 7637–7652.
- (93) Agarwal, P.; Kim, S. A.; Archer, L. A. Crowded, confined, and frustrated: dynamics of molecules tethered to nanoparticles. *Phys. Rev. Lett.* **2012**, *109*, No. 258301.
- (94) Kim, S. A.; Mangal, R.; Archer, L. A. Relaxation Dynamics of Nanoparticle-Tethered Polymer Chains. *Macromolecules* **2015**, *48*, 6280–6293.
- (95) Matsumiya, Y.; Inoue, T.; Oishi, Y.; Watanabe, H. Orientational anisotropy of bead-spring star chains during creep process. *J. Polym. Sci., Part B: Polym. Phys.* **2006**, 44, 3501–3517.

Supporting Information

The effects of asymmetric molecular architecture on chain stretching and dynamics in miktoarm star copolymers

Thomas Kinsey¹, Emmanuel Urandu Mapesa¹, Weiyu Wang², Kunlun Hong^{1,2}, Jimmy Mays³, S. Michael Kilbey II, Joshua Sangoro^{1*}

¹Department of Chemical and Biomolecular Engineering, University of Tennessee, Knoxville, TN 37996, United States

²Center for Nanophase Materials Science, Oak Ridge National Laboratory, Oak Ridge, TN 37831, United States

³Department of Chemistry, University of Tennessee, Knoxville, TN 37996, United States

Contents

Part A: Analysis of structural data
A.1: TEM imagesS2
A.2: SAXS Profiles of PS ₂ PI ₂ S3-S4S3-S4
A.3: Calculating Scattering InvarianceS4-S6
Part B: Analysis of the dielectric loss spectra
B.1: Havriliak Negami Fitting and Master CurvesS7-S12
B.2: Segmental Relaxation Spectral Shape and Relaxation RatesS12-S14
B.3: Comparison with Data from LiteratureS14-S16
Part C: Details on the Gaussian chain and the Kirkwood correlation factorS17-S18

Part A: Analysis of structural data

A.1: TEM images

TEM images for the $18k-32k_2$ and $18k-18k_2$ polymers were taken to confirm the microstructures suggested by the SAXS profiles. For all of the other miktoarm copolymers, there was not such ambiguity in determining the structure from SAXS profiles, and therefore, only these two polymers were imaged. The samples for TEM were prepared in the same way as for SAXS, except rather than sandwiching the annealed films between Kapton tape, cross sections of the $100\mu m$ films were cut into $\sim 100 nm$ sections using cryo-ultramicrotome at 90° C, collected onto 400 copper mesh TEM grids and standed with vapors of aqueous $0sO_4$ (4wt%) for three hours. The images were taken at the Joint Institute for Advanced Manufacturing at the University of Tennessee Cherokee Farms Campus with a Zeiss Libra 120 TEM. The images are in Figure S1.

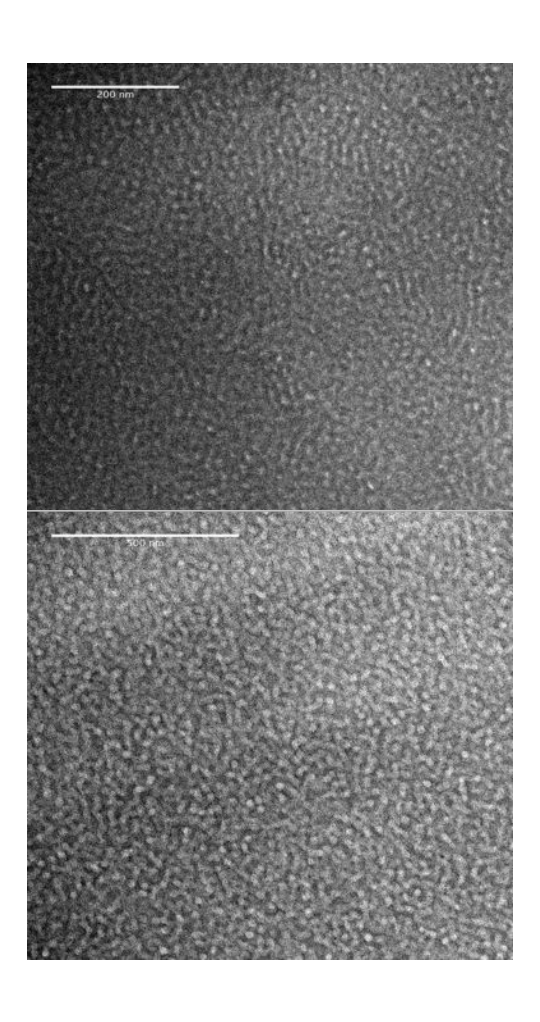


Figure S1: TEM images of PS phases (white) and continuous OsO_4 -stained PI domain (dark) for the $18k18k_2$ polymer which shows cylinders and spheres of PS (a) and $18k32k_2$ which shows PS spheres (b).

A.2: SAXS profiles of the PS₂PI₂ polymers

Small angle x-ray scattering measurements (SAXS) supported by transmission electron microscopy (TEM) images were taken to determine the structural lengthscales of phase separation formed by the miktoarm star copolymers in this study. SAXS profiles for the 3-arm miktaorm copolymers are found in Figure 1 in the main text. Figure S1 shows the SAXS intensity profiles plotted against the scattering vector $\mathbf{q} = 4\pi \sin(\theta) \lambda^{-1}$, where θ is the scattering angle and λ is the wavelength of the insident x-ray). The q values for the observed peaks are displayed in the figure. The scattering for 18k-10k2 and 16k-24k2 copolymers correspond to lamellar structure. These data were published previously, and used with permission.³ The $16k_2$ - $9k_2$ polymer forms ~ 10.6 nm PI spheres within a continuous PS domain using the equation noted in the main text. As per the 2D SAXS profile in Figure S2, these PI spheres are prefferentially oriented with repect to the x-ray beam. For the 16k₂- $52k_2$ copolymer, the q_1 value of the higher order peak is $\sim \sqrt{3}$ q* suggesting domains of PS cylinders within a continuous PI matrix. Lastly, the PI block molecular weight dependence of the q* values are plotted in Figure S3 where these values are observed to decrease with increasing block molecuar weight for all polymers, and decrease faster for the 4-arm miktoarm copolymers.

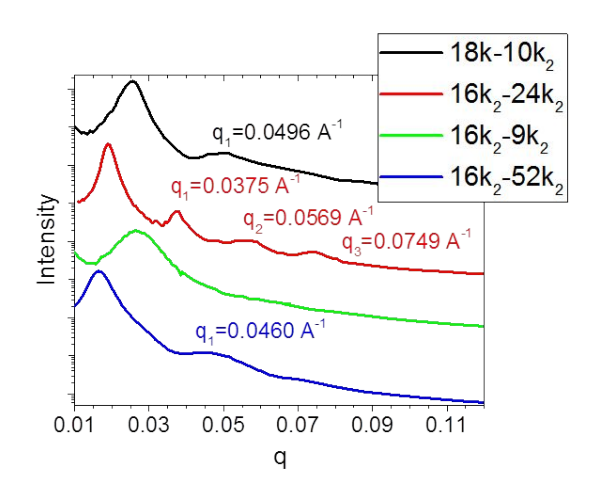


Figure S2: SAXS Profiles for the 4-arm miktoarm polymers and the $18k-10k_2$ polymer which is also found in Fig. 1 of the main text. Q* peaks for the $18k10k_2$, $16k_224k_2$, $16k_29k_2$ and $16k_252k_2$ polymers occur at 0.0256 A⁻¹, 0.0194 A⁻¹, 0.0263 A⁻¹, and 0.0164 A⁻¹, respectively. Higher order peaks are noted in the figure with colors corresponding to the respective data.

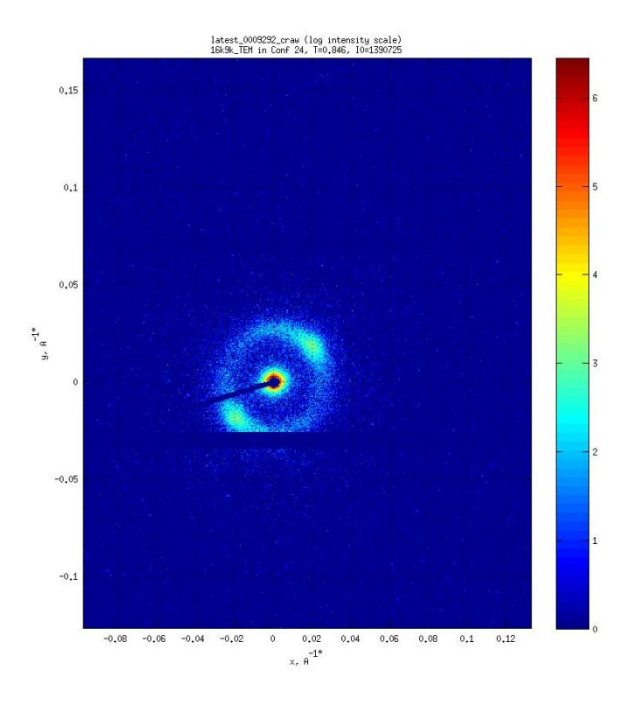


Figure S3: 2D scattering profile for the $16k_2$ - $9k_2$ polymer. The nonuniform scattering in all directions suggest that the spherical domains are preferentially ordered with respect to surface normal to the incident beam.

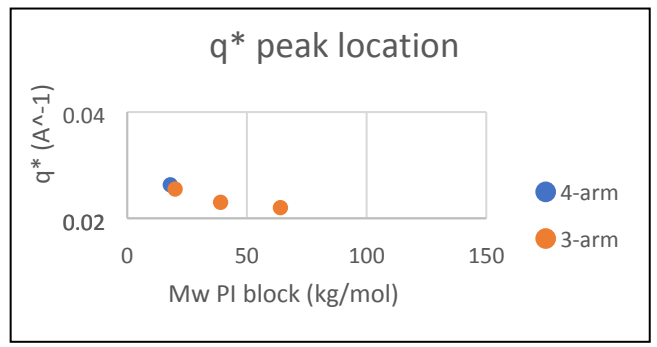


Figure S4: q values for the lowest Bragg peak (q^*) for all miktoarm polymers *versus* the molecular weight of the PI block.

A.3: Calculating the Scattering Invariance

Different regions of SAXS profiles afford different information about the size and shape of the relative electronic structures that scatter the incident beam. At the high q values, also known as the Porod region, information regarding the interfaces of domains can be determined. The Kratky plot, displayed for all of the miktoarm polymers in Figure S5, is typically used in biological systems for disorder in protein folding.⁴ However, for analysis of phase separated block copolymers, the integration of this data over all q gives the scattering invariance, Q, which is relative to the change in electron density across the interface. Value of Q are shown for each miktoarm star copolymer in Table S1. The $18k(12k-3k')_2$ and $18k10k_2$ polymers have the highest Q value of these polymers and shows that the relative change in electron density is sharpest for these two polymers compared to the others. Integration was performed numerically on the Kratky-plot data using OriginPro software; that is to say, the data was not fit with any function prior to integration.

Another representation of the SAXS data is the Porod plot which is I(q) q^4 vs q^4 which is shown in Figure S6. The limit as $q\to\infty$ of this data give a relative estimate of the thickness of the domain interphase.⁴ Here, the $18k(12k-3k')_2$ and $18k10k_2$ polymers have lower values at high-q, which correspond to a relatively narrow interfacial thickness. The ratio of $[\log_{q\to\infty}I(q)\ q^4]\ Q^{-1}$ gives the relative surface area to volume ratio of the interface. Since the $18k(12k-3k')_2$ and $18k10k_2$ polymers have the highest Q values and lowest values at high-q in the Porod plot of all the polymers, and these values are similar for these two polymers, these two polymers have similarly sharp interfaces (*i.e.* highest interfacial surface area to volume ratio) between the PS and PI domains. In the main text, this result supports that there is sufficient phase separation between the PS and PI domains for the $18k(12k-3k')_2$, and that the PS' block is not mixed with the PI domain.

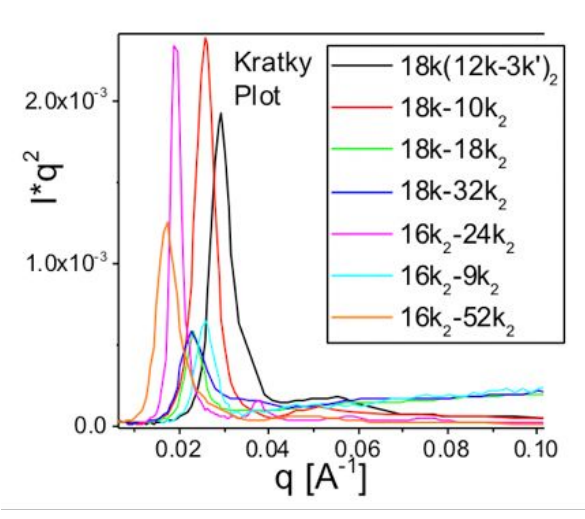


Figure S5: Kratky plot of the scattering data for all miktoarm star copolymers. Integration of these data give the scattering invariant and is a relative estimate of electron density change.

Table S1: SAXS Invariance				
Sample	Q (a.u. Å ³) = $\int_{0.01}^{0.1} I(q)q^2 dq$			
18k(12k-3k')2	1.68E-05			
18k-10k2	1.65E-05			
18k-18k2	1.00E-05			
18k-32k2	8.84E-06			
16k2-24k2	6.09E-06			
16k2-9k2	3.90E-06			
16k2-52k2	3.83E-06			

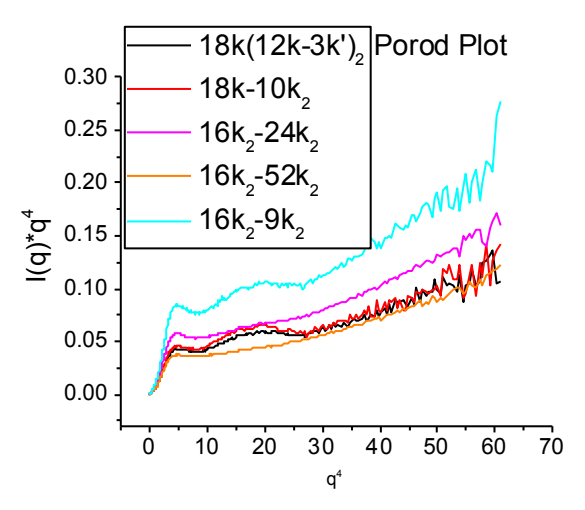


Figure S6: The Porod Plot of the SAXS profiles for miktoarm polymers. Limit of I(q) q^4 at high q values is associated with the relative thickness of the scattering interface. Smaller values at high q values correspond to decreased thickness of the interphase.

Part B: Analysis of the dielectric loss spectra

B.1: Havriliak Negami Fitting and Master Curves

All of the dielectric data for the miktoarm star copolymers (except for the PS(PI-PS')₂ polymer and $16k_2$ - $52k_2$ polymer, see Fig. S10 and S11, respectively) were initially analyzed by creating mastercurves with a reference temperature by shifting the dielectric loss data at each temperature (240K-330K) by a shift factor aT.⁵ The temeprature dependent shift factors for the 3-arm miktoarm star polymers are displayed in Figure S7. The shift factors for the 4-arm systems follows that for the linear diblock system (solid line in Fig. S7). The resulting master curves are displayed in Figure S8. This representation shows that the frequency-temperature superposition principle holds for all of these systems. The analysis of the mastercurves allows the segmethal and chain relaxations to be fit over a wide frequency range, and suggest the spectral shapes (not necissarily intensity) of both relaxtions are constant with temperature within the temperature range. Then, when fitting the imaginary permittivity ε'' spectra at individual temperatures, the variables of the fitting parameters in the Havriliak Negami (HN) function used for each relaxation peak (Eqn. S1) can be constrained rather than letting the parameters fit freely with OriginPro analysis software.

$$\varepsilon^*(\omega) = \varepsilon_{\infty} + \frac{\Delta \varepsilon_{HN}}{(1 + (i\omega \tau_{HN})^{\alpha})^{\beta}}$$
 (S1)

The variables in the HN function are $\Delta \varepsilon_{HN}$, τ_{HN} , α and β , which are the dielectric strength of the relaxation, the relaxation rate, and symmetric and asymmetric stretching parameters (e.g. shape parameters), respectively. The ω (=2 π f) is the angular frequency of the applied electric field, ε_{∞} is the high frequency value of the real part of the complex permittivity ε^* . For the segmental relaxation, $\Delta \varepsilon_{HN}$ and τ_{HN} are termed $\Delta \varepsilon_{\alpha}$ and τ_{α} , respectively. For the chain relaxation, $\Delta \varepsilon_{HN}$ and τ_{HN} are termed $\Delta \varepsilon_{n}$ and τ_{n} , respectively. The fitting parameters for all miktoarm star copolymers in this study are in the Table S2. The segmental and chain relaxations are fit with a linear combination of two HN functions and at higher temperatures

and with a low frequency contribution to the spectra is added to describe dc conductivity using $\varepsilon'' = \sigma_0(2\pi f \varepsilon_0)^{-1}$ where σ_0 is the dc conductivity, ε_0 is the vacuum permittivity and f is frequency in Hz. This contribution is subtracted from the higher temperature spectra for each miktoarm copolymer. At higher frequencies, the overlap of the chain and segmental relaxations was analyzed such that the subtraction of the HN function for the PI α -relaxation results in a high frequency Debye-like cut-off of the chain relaxation in accordance with negligible cross-correlations between the μ^{\parallel} and μ^{\perp} in Eq. 2 of the main text. For such low ε'' intensities of the chain relaxation at frequencies that overlap with the α relaxation, the shape of each relaxation is not affected by subtraction of an HN function fit to the corresponding dielectric process.

Equation S2 is used calculate the rate of maximum loss ($\omega_{\alpha, max}$ or $\omega_{n, max}$) for corresponding HN fits to the α or chain relaxation, respectively using the fitting parameters from Eqn. S1.

$$\omega_{n, max} = \tau_{HN}^{-1} \left[\frac{\sin(\alpha \beta \pi/2) + 2\beta}{\sin(\alpha \pi/2) + 2\beta} \right]^{1/\alpha}$$
 (S2)

The chain relaxation for the $18k(12k-3k')_2$ has a temperature dependent shape, and, therefore, a mastercurve could not be prepared from the dielectric data. Consequently, the chain relaxation was fit individually for each temperature without an initial estimate of the shape parameters. The segmental relaxation shape was kept constant and the fits at four temperatures with segmental relaxation HN fit subtracted from the data are shown in Figure S10. Also, to confirm the relaxation rates, the Kramers-Kronig relation is used to calculate the dielectric loss data from the real part of the complex permittivity by $-2/\pi$ [$d \epsilon'/d \log \omega$] which suppresses the high-temperature, low-frequency conductivity contribution, and the frequency of maximum loss is determine without and HN fit. This is also performed for the dielectric data from the $16k_2$ - $52k_2$ polymer to confirm the chain relaxation rates that are not visible due to conductivity contributions to the spectra (see Figure S11). These relaxation rate data agree with the rates determined from Eqn. S2.

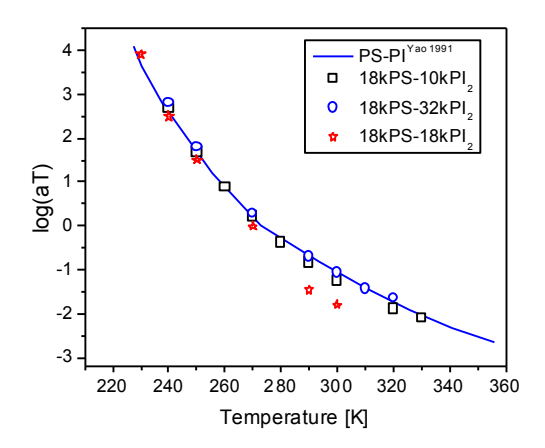


Figure S7: Frequency-temperature superposition shift factors at each temperature for the three 3-arm miktoarm star polymers in this study. The aT are similar to that observed previously for lamellar forming PS-PI linear diblock copolymers⁵.

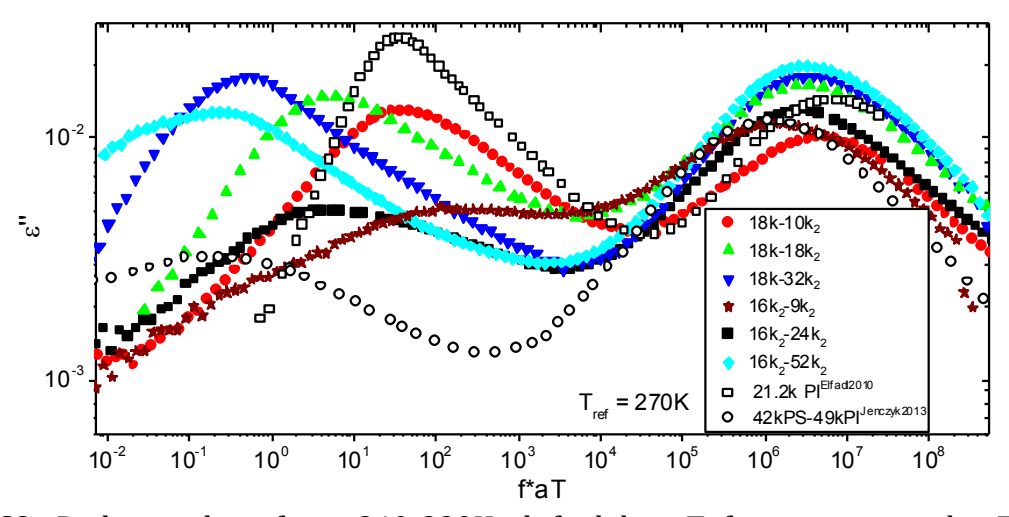


Figure S8: Dielectric loss from 240-330K shifted by aT factor to give the Frequency Temperature Superposition representation for all miktoarm polymers, and a linear diblock copolymer² (lamellar) and PI homopolymer¹ from the literature. The reference temperature of 270K is used with aT values taken from those used for PI homopolymer⁵ or from Fig. S7

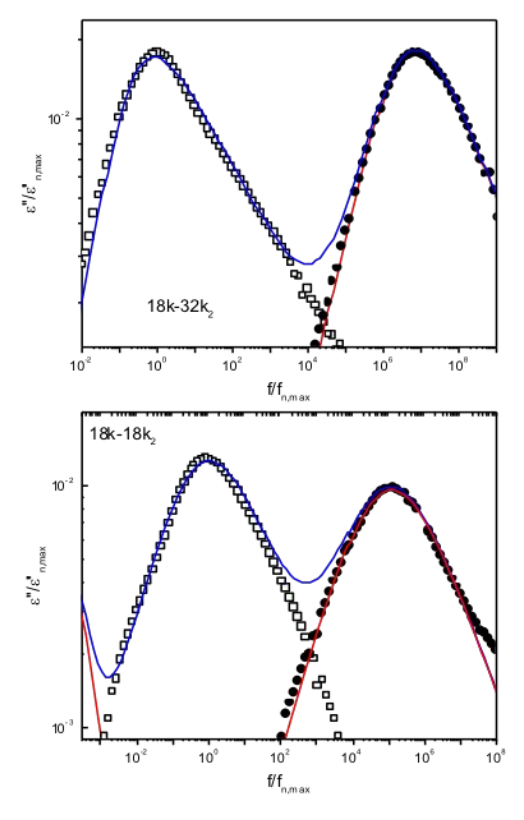


Figure S9: Analyses of the dielectric loss in the frequency-temperature-superposition representation for the $18k-32k_2$ (top) and $18k-18k_2$ (bottom) miktoarm polymers are performed by fitting the chain and segmental relaxations (low and high frequencies, respectively) each with the empirical Havriliak-Negami function (Eq. S1). First, the segmental relaxation is fit with a HN function (red line). This data was then subtracted from the spectrum to reveal the shape of the dielectric chain relaxation (open squares). This chain relaxation is then also fit with a HN function. A linear combination of the two HN fits are observed as the blue line. Subtracting this chain relaxation HN fit from the data reveals the segmental relaxation (closed circles).

TABLE S2: Shape parameters for HN fit functions (Eqn S1) to the loss spectra in Fig. S8

Polymer ID	α (segmental)	β (segmental)	α (chain)	β (chain)	
16k ₂ -9k ₂	$0.54 (\pm 0.02)$	$0.71 (\pm 0.02)$	$0.34 (\pm 0.02)$	$0.96 (\pm 0.02)$	
16k ₂ -24k ₂	$0.65 (\pm 0.03)$	$0.6 \ (\pm 0.03)$	$0.58 (\pm 0.03)$	$0.26 (\pm 0.03)$	
16k ₂ -52k ₂	$0.62 (\pm 0.04)$	$0.68 (\pm 0.04)$	See Fig. S10		
18k-10k ₂	$0.63 (\pm 0.02)$	$0.59(\pm 0.02)$	$0.54 (\pm 0.03)$	$0.75 (\pm 0.03)$	
18k-18k ₂	$0.58 (\pm 0.05)$	$0.75 (\pm 0.05)$	$0.55(\pm 0.02)$	$0.7 \ (\pm 0.02)$	
18k-32k ₂	$0.65(\pm 0.04)$	$0.6 \ (\pm 0.04)$	$0.63 (\pm 0.05)$	$0.78 (\pm 0.05)$	
18k(12k-3k') ₂	$0.63 (\pm 0.03)$	$0.58 (\pm 0.03)$	See Fig. S11		

*The error shown is the standard error from OriginPro least-squares Levenberg-Marquardt algorithm for a χ^2 tolerance value of 10^{-9} .

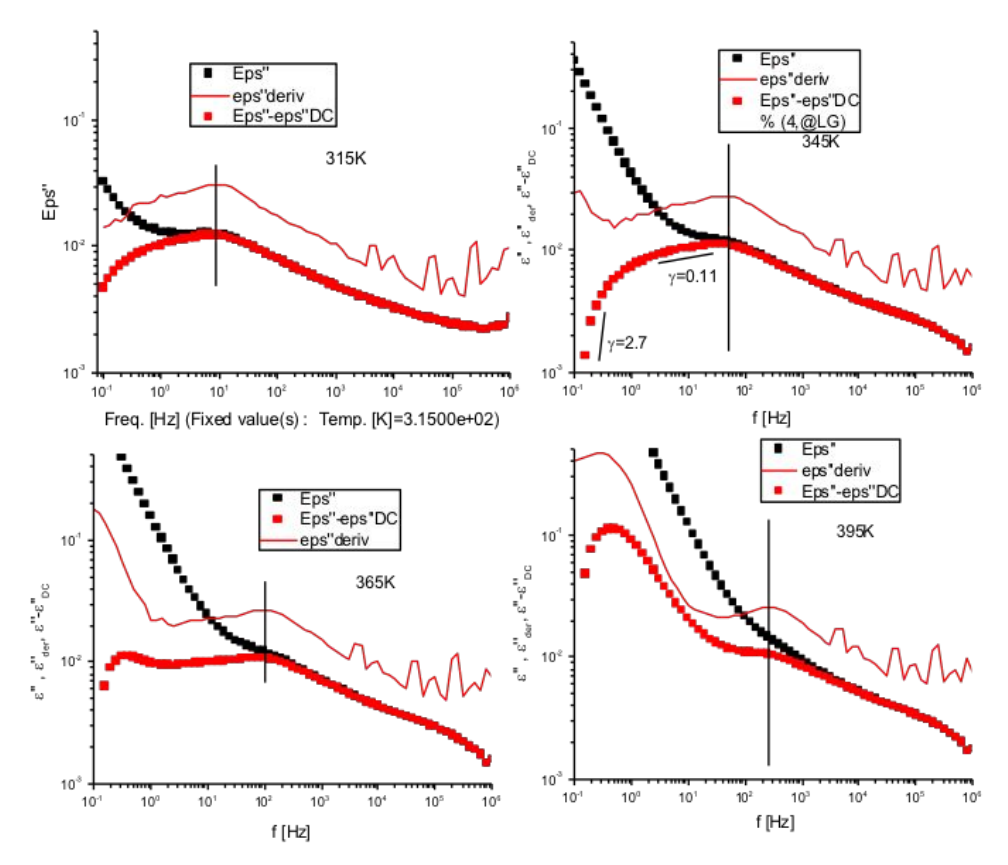


Figure S10a-d: To determine the higher temperature chain relaxation rates, the dielectric loss (black squares) spectra at four different temperatures (a-d, identified on the plot) are shown for the $16k_2\text{-}52k_2$ polymer. While the FTS principle holds, the peak maximum of the chain relaxation is difficult to observed due to a strong interfacial polarization process toward low frequencies (described by $\epsilon'' = \sigma_0(2\pi f\,\epsilon_0)^\text{-1})$ which is subtracted from the data (red squares). In addition to subtracting the conductivity contribution, the frequency of maximum loss for the chain relaxation is more clearly observed when calculating the ϵ'' from the Kramers-Kronig relation (red line) through $\epsilon''_{\text{der}} = -2\pi^{-1}\frac{d\epsilon'}{d\ln\omega}$.

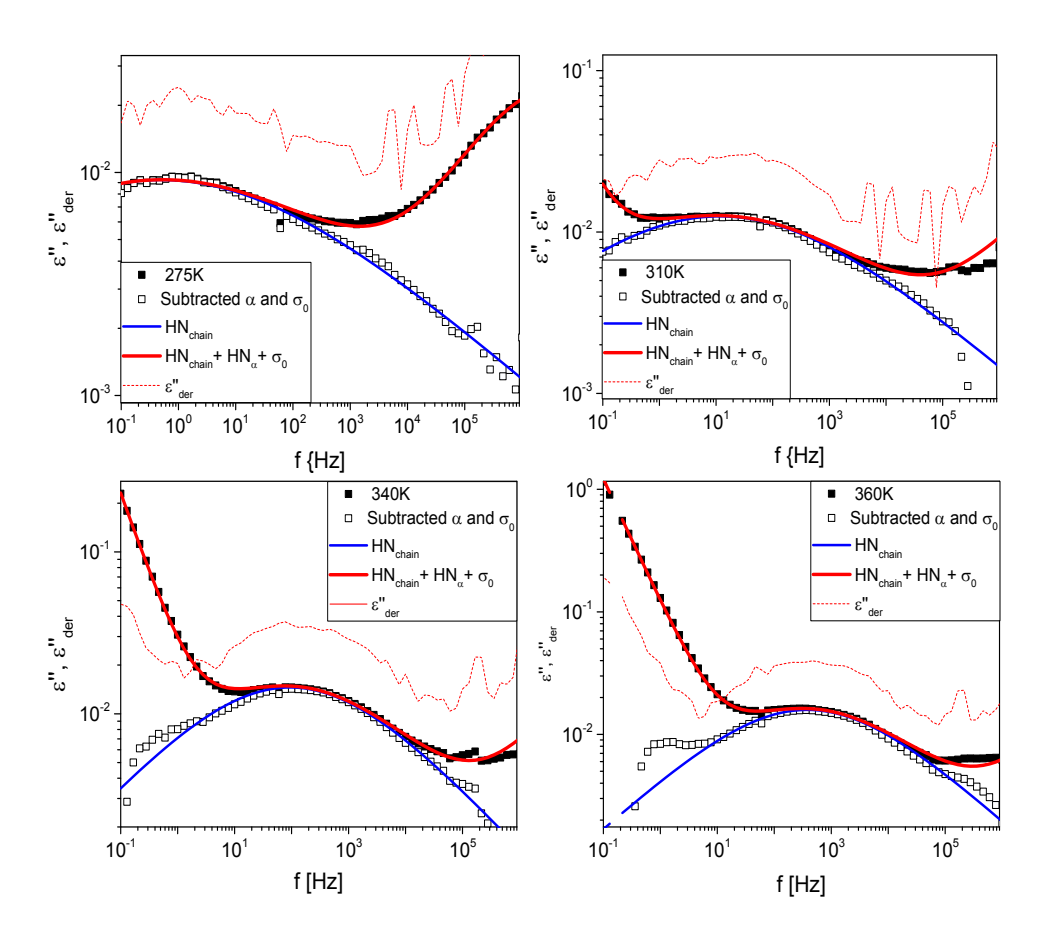


Fig S11a-d: Dielectric loss at four temperatures for the $18k(12k-3k')_2$ polymer (filled squares). The HN fits for the chain relaxation is observed as a blue line. The contribution to the spectrum at higher frequencies (segmental relaxation) and lower frequencies (conductivity) are fit with a HN function and with $\varepsilon'' = \sigma_0(2\pi f \varepsilon_0)^{-1}$, respectively. The fits for these contributions are subtracted from the data revealing the chain relaxation (open squares) to show the accuracy of the chain relaxation HN fit. The dotted red line is the ε'' representation calculated from the Kramers-Kronig relation ($\varepsilon''_{\rm der} = -2\pi^{-1} \frac{d\varepsilon'}{d \ln \omega}$) which suppresses conductivity contributions to the loss spectra. Each temperature was fit individually due to the change in the spectral shape of the chain relaxation as described in the main text.

B2: Segmental relaxation spectral shape and relaxation rates

In this section the relaxation rates are plotted against temperature for the PI segmental relaxation in Figure S12a and for the PI chain relaxation in Figure S13. In Figure S12b, the initial HN fits for the PI chain relaxation to the master curve data in Figure S8 are subtracted from the spectrum, then the data is normalized by the ε'' peak value and the

frequency of that value. This allows the shapes of this relaxation to be compared qualitatively. The similarity in this relaxation shape and in the relaxation rates in Figure S12a confirm that all PI segments exist in similar localized environments with the same local friction coefficient (analogous to the local friction of chains Eqn. 4 in the main text). Of the relaxation rate data in Figure S13 are fit with the Vogel-Fulcher-Tammann (VFT) equation, excluding that for the $18k(12k-3k')_2$ polymer which follows an Arrhenius temperature dependence. The equations for these fits are found in the footer of Table S3. Table S3 shows the VFT fit parameters for these polymers. The vertical line in Figure S13 corresponds to T = 320K. The rates at this temperature are plotted against PI arm molecular weight in the main text.

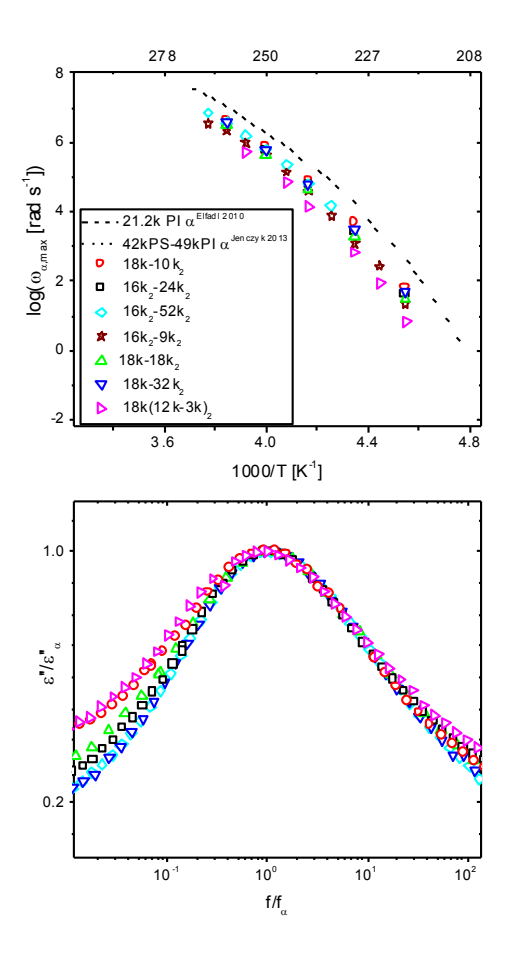


Figure S12: Segmental (α -) relaxation rates of PI plotted for all miktoarm star polymers in this study (top). Additionally, the α relaxation rates for the PI homopolymer and PI in a lamellar forming PS-PI linear diblock copolymer are included from the literature¹⁻². The PI dielectric loss corresponding to the α relaxation is normalized by maximum loss and frequency for all miktoarm star polymers displaying similar spectral shapes. This implies a similar distribution in relaxation times for this process, and that all PI segments have the same local frictions for this segmental motion.

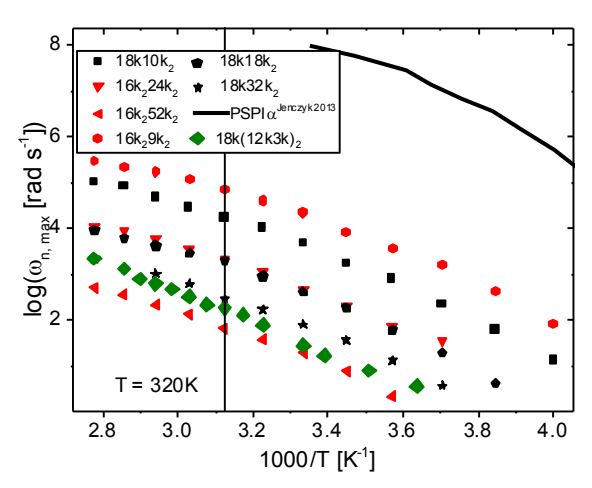


Figure S13: Normal mode relaxation rates plotted versus inverse temperature for all miktoarm polymers investigated. Segmental relaxation rates for PI in a lamellar forming PS-PI diblock copolymer from literature is included for reference (solid line). These data were fitted with Vogel-Fulcher-Tammann equation and the resulting parameters are shown in Table S2 below.

Table S3: VFT/Arrhenius fit parameters to data in Fig. S13					
Sample	b		$m (-E_a/R)$		
18k(12k-3k') ₂		12.56	-3.31		
Sample	T_0		ω_{∞}	В	
18k-10k ₂		156.5	2.61E+08		1570
18k-18k ₂		183.5	3.51E+06		1043
18k-32k ₂		168.0	2.90E+06		1379
16k2-9k ₂		170.0	1.30E+08		1137
16k ₂ -24k ₂		151.0	3.83E+07		1668
16k ₂ -52k ₂		186.0	2.84E+05		1098

VFT eqn: $\log (\omega_n) = \log (\omega_\infty) + B (T-T_0)^{-1}$ Arrhenius eqn: $\log (\omega_n) = b + m T^{-1}$

B.3: Comparison with Data from Literature

As discussed in the main text the PI chain relaxation spectral shape is known to change with morphology for PS-PI systems due to varied local constraints on chain motion among different geometries. In Figure S14, the PI chain relaxation spectral shapes of the 4arm miktoarm star polymers are shown by dividing the dielectric loss by the PI block volume fraction (ϕ_{Pl}) and the frequency by the frequency of maximum loss (f_n) . In this way the intensities and shapes of these chain relaxations are observed to vary with morphology by changing the molecular weight of the PI block. Qualitatively these changes follow that observed for the linear PS-PI diblock system. As shown in Figure S15, the chain relaxations of the $16k_29k_2$ and $16k_2-52k_2$ polymers from Figure S14 are compared to chain relaxations of PI in linear diblock copolymers that are reported to form similar morphologies. The intensities relative to the ϕ_{Pl} and the relaxation shape are observed to be similar and suggest that the symmetric architecture of the PS₂PI₂ polymer has a similar effect on the PI chain relaxations across various morphologies as in the linear diblock systems, as discussed in detail in the main text. Lastly, we only found one other publication that measures the dielectric chain relaxation for miktoarm star copolymers. Data from the paper by Floudas et. al in 1996 is reproduced in Figure S16 and shown to have a similar relaxation shape as the PI chain relaxation in our PSPI₂ polymers.⁶

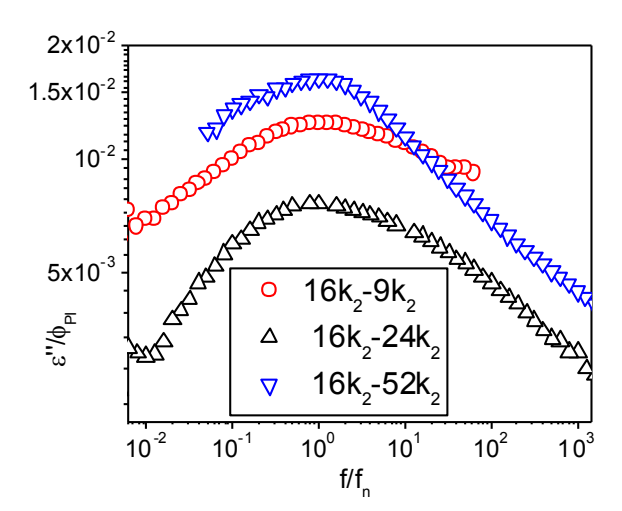


Figure S14: Dielectric loss spectra of PI chain relaxations normalized by PI volume fraction (ϕ_{PI}) for the three 4-arm miktoarm polymers (PS_2PI_2) in our study.

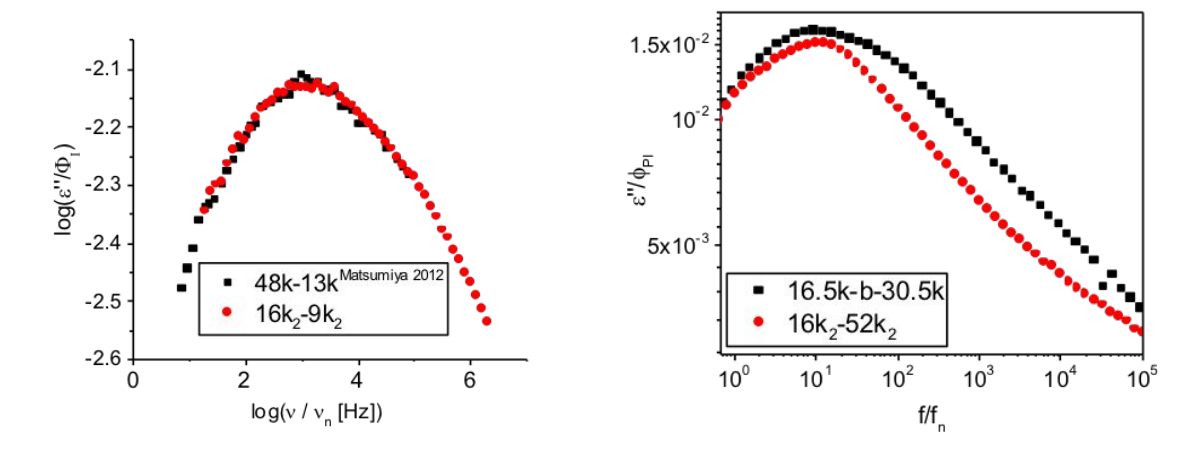


Figure S15: Normalized dielectric loss corresponding to chain relaxations for $16k_2$ - $9k_2$ miktoarm polymer compared with that for a PI-sphere forming linear PS-PI diblock (Left)⁷, and for $16k_2$ - $52k_2$ miktoarm polymer compared with a linear PS-PI diblock with similar continuous PI domain that we measured ourselves (Right).

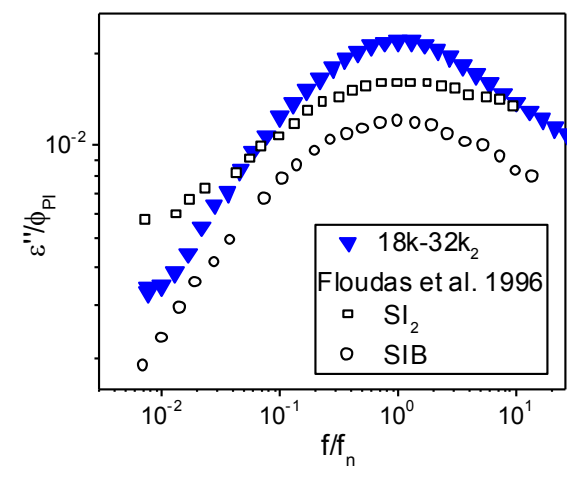


Figure S16: One other publication reports dielectric loss chain relaxation spectra of a miktoarm star copolymers of $PSPI_2$ architecture, where SI_2 is the same as our $PSPI_2$ architecture with $Mw_{PS} = 7.6$ kg/mol and $Mw_{PI, arm} = 8$ kg/mol and SIB has one PI arm replaced by polybutadiene. Here the chain relaxation normalized by the PI volume fraction for our $18k-32k_2$ polymer is compared against that for the similar $PSPI_2$ polymer, and a miktoarm star terpolymer with one arm of polystyrene, one arm of poly(cis-1,4-isoprene) and one arm of polybutadiene. The similarity in spectral shapes of this chain relaxation is in agreement with our data and discussion in the main text.

Part C: Details on the Gaussian chain and the Kirkwood correlation factor

Regarding the Free Energy of the Gaussian Coil for Block Copolymers in terms of the Kirkwood-Fröhlich factor as calculated by Watanabe⁸:

The free energy (F) of a phase separated block copolymer system is increased compared to that described by the homopolymer Gaussian coil in order to maintain the order of phase separation. Two additional contributions to F are the interfacial energy (i.e. excess energy compared to the homopolymer required to maintain the interface) and energy of chain stretching (i.e. excess energy from the Gaussian coil due to orientational anisotropy). These two additional terms are counterbalanced in order to minimize F at equilibrium.

Matsen describes the free energy of an incompressible, lamellar forming block copolymer system as

$$\frac{F}{nk_BT} = \Sigma \rho_0 a \left(\frac{\chi}{6}\right)^{1/2} + \sum_{blocks} \frac{\pi^2 N}{8\Sigma^2 \rho_0^2 a^2}$$
 (S2)

where n is the number of molecules, k_B is the Boltzmann constant, T is absolute temperature, Σ is the interfacial area per molecule (Σ =A/n, with A as the interfacial area), ρ_0 is the segment density, a is the statistical segment length, χ is a proportionality constant equivalent to the Flory-Huggins interaction parameter and N is the total number of segments in the polymer block⁹. Note this is very similar to Watanabe's use of the Zhulina-Halperin self-consistent field theory model for lamellar ABA triblock copolymers¹⁰. The first term represents the free energy of the interface, which is analogous to the free energy of mixing. The second term is the chain stretching energy, which is also termed the elastic free energy, and can be split into a sum of the two individual blocks for a diblock system. To minimize the total free energy, there is a counterbalance between a large Σ that minimizes the stretching energy and a small Σ which minimizes the interfacial energy. It has been determined that the 3-arm miktoarm system has an increased area per molecule at the interface which corresponds to a reduced chain stretching portion of the total free energy. The equilibrium area per molecule is determined at the minimum of the total free energy in Eq S2 below.

$$\Sigma = \frac{N^{1/2}}{\rho_0 \alpha^2} \left(\frac{3\pi^4}{8\chi N}\right)^{1/6} \tag{S3}$$

Substituting Eq. S3 into Eq. S2 shows that the equilibrium stretching energy is half the equilibrium interfacial energy. It has been determined that the asymmetric architecture of the AB_n miktoarm polymers have an increased χ parameter and an increased area per molecule. Therefore, from Eqs. S1 and S2 there is a decreased stretching energy in the architecturally asymmetric systems compared in the to block copolymers with symmetric architectures. This is represented in the dielectric loss spectra as a more homogeneous distribution of chain relaxation times as explained in the main text.

In describing the Kirkwood-Fröhlich factor, g, Watanabe considers an additional initial orientational anisotropy (S_0) due to subchain tension after some strain, γ , for entangled chains. For incoherent subchains (g=1) after some strain $S_0=\gamma/3$, which describes the initial orientational anisotropy of non-entangled homopolymers. For coherent subchains (g=4/5) after some strain $S_0=4\gamma/15$ and describes the orientational anisotropy of entangled homopolymers that have a slight increase in anti-parallel orientations amongst chains (0 < g < 1 for antiparallel orientations). If we consider the subchain tension in entangled chains to be comparable to the stretching energy in block copolymers, it is logical that there would be an decrease in orientational anisotropy of subchains for the stretched chains of the $18k(12k-3k')_2$ polymer (g=1/3) to have an ani-parallel orientation of neighboring chains. The increased chain stretching energy then corresponds to a decreased interfacial energy that allows for motion of the junction point between the PS block with the two PI chains in the PS(PI-PS')₂ polymer.

References

- 1. Elfadl, A.; Kahlau, R.; Herrmann, A.; Novikov, V. N.; Rössler, E. A., From Rouse to Fully Established Entanglement Dynamics: A Study of Polyisoprene by Dielectric Spectroscopy. *Macromolecules* **2010**, *43* (7), 3340-3351.
- 2. Jenczyk, J.; Dobies, M.; Makrocka-Rydzyk, M.; Wypych, A.; Jurga, S., The segmental and global dynamics in lamellar microphase-separated poly(styrene-b-isoprene) diblock copolymer studied by 1H NMR and dielectric spectroscopy. *European Polymer Journal* **2013**, *49* (12), 3986-3997.

- 3. Kinsey, T.; Mapesa, E. U.; Wang, W.; Hong, K.; Mays, J.; Kilbey, S. M.; Sangoro, J., Impact of Molecular Architecture on Dynamics of Miktoarm Star Copolymers. *Macromolecules* **2018**, *51* (14), 5401-5408.
- 4. Boldon, L.; Laliberte, F.; Liu, L., Review of the fundamental theories behind small angle X-ray scattering, molecular dynamics simulations, and relevant integrated application. *Nano Rev* **2015**, *6*, 25661.
- 5. Yao, M. L.; Watanabe, H.; Adachi, K.; Kotaka, T., Dielectric relaxation behavior of styrene-isoprene diblock copolymers: bulk systems. *Macromolecules* **1991**, *24* (10), 2955-2962.
- 6. Floudas, G.; Hadjichristidis, N.; Iatrou, H.; Pakula, T., Microphase Separation in Model 3-Miktoarm Star Co- and Terpolymers. 2. Dynamics. *Macromolecules* **1996**, *29*, 3139-3146.
- 7. Matsumiya, Y.; Chen, Q.; Uno, A.; Watanabe, H.; Takano, A.; Matsuoka, K.; Matsushita, Y., Dielectric behavior of Styrene–Isoprene (SI) Diblock and SIIS Triblock Copolymers: Global Dynamics of I Blocks in Spherical and Cylindrical Domains Embedded in Glassy S Matrix. *Macromolecules* **2012**, *45* (17), 7050-7060.
- 8. Watanabe, H., Slow Dynamics in Homopolymer Liquids. *Polymer Journal* **2009**, *41* (11), 929-950.
- 9. Matsen, M. W., The standard Gaussian model for block copolymer melts. *Journal of Physics: Condensed Matter* **2002**, *14* (2), R21-R47.
- 10. Watanabe, H.; Tan, H., Dielectric Investigation of Bridge Fraction in Triblock/Diblock Mixed Lamella. *Macromolecules* **2004**, *37* (13), 5118-5122.